The atmospheric HCHO budget at Dumont d'Urville (East Antarctica): Contribution of photochemical gas-phase production versus snow emissions

Susanne Preunkert,[1] Michel Legrand,[1] Guillaume Pépy,[1] Hubert Gallée,[1] Anna Jones,[2] and Bruno Jourdain [1]

Received 18 March 2013; revised 11 November 2013; accepted 18 November 2013; published 12 December 2013.

[1] HCHO was monitored throughout the year 2009 at the coastal East Antarctic site of Dumont d'Urville (DDU) using Aerolaser AL-4021 analyzers. The accurate determination of less than 100 pptv required optimization of the analyzers, in particular, to minimize effects of changing ambient temperatures. The impact of station activities and of the presence of large penguin colonies at the site in summer was scrutinized. The obtained contamination-free record indicates monthly means close to 50 pptv from May to September and a maximum of 200 pptv in January. Zero-dimensional and 2-D calculations suggest that in summer, the largest HCHO source is the gas-phase photochemistry (80%) mainly driven by methane oxidation, which is considerably greater than from snow emissions (20%). The influence of light alkenes, dimethyl sulfide, and halogens remains weak. In winter, snow emissions represent the main HCHO source (70%). These findings are compared to previous studies conducted at the West Antarctic coast. It is shown that in summer the HCHO production from methane chemistry is 3 times more efficient at DDU than at the west coast due to more frequent arrival of oxidant-rich air masses from inland Antarctica. Halogen chemistry is found to represent a weak HCHO sink at both West and East Antarctica. Compared to DDU, the shallower atmospheric boundary layer and the less efficient gas-phase production at the west coast make the snow pack the dominant HCHO source (85%) compared to gas-phase photochemistry (15%) there in summer.

Citation: Preunkert, S., M. Legrand, G. Pépy, H. Gallée, A. Jones, and B. Jourdain (2013), The atmospheric HCHO budget at Dumont d'Urville (East Antarctica): Contribution of photochemical gas-phase production versus snow emissions, *J. Geophys. Res. Atmos.*, *118*, 13,319–13,337, doi:10.1002/2013JD019864.

1. Introduction

[2] Formaldehyde (HCHO) is produced within the atmosphere during the oxidation of numerous hydrocarbons emitted by anthropogenic and natural sources and also directly emitted by combustion. Satellite observations clearly reveal the importance of sources like isoprene oxidation over forested areas, biomass burning over the tropics, and anthropogenic emissions over very populated regions [*Wittrock et al.*, 2006; *Stavrakou et al.*, 2009]. In the remote troposphere, HCHO is thought to be mainly produced by the photooxidation of CH_4, the most abundant atmospheric hydrocarbon [*Lowe and Schmidt*, 1983].

[3] With mixing ratios up to 10 to 50 ppbv in megacities [*Grutter et al.*, 2005], HCHO is intensively monitored in polluted areas because of its carcinogenic effect [*Hauptmann et al.*, 2003]. In the remote marine boundary layer, mixing ratios of 200 pptv [*Wagner et al.*, 2001] and 300 pptv [*Ayers et al.*, 1997] were observed at low and middle southern latitudes, respectively.

[4] At higher latitudes, studies were conducted over the Arctic and Antarctic snowpack aiming to evaluate (1) to what extend HCHO can be used as an ice core proxy for changes in the oxidative capacity of the atmosphere over the past and (2) whether the snowpack represents a major formaldehyde source for the atmospheric polar boundary layer [*Sumner and Shepson*, 1999; *Yang et al.*, 2002; *Jacobi et al.*, 2002; *Hutterli et al.*, 2004]. In addition, to understand the HCHO budget of the background troposphere in very remote regions, year-round studies were conducted at the Neumayer (NM) [*Riedel et al.*, 1999] and Halley (HA) [*Salmon et al.*, 2008] sites, both located in coastal Antarctica. The two records captured a well-marked seasonal cycle but with different absolute HCHO levels (390 pptv at NM against 130 pptv at HA in January, for instance). *Salmon et al.* [2008] emphasized that whereas there are no striking geographical and climatological differences between the two coastal sites

[1]CNRS/UJF–Grenoble 1, Laboratoire de Glaciologie et Géophysique de l'Environnement, Grenoble, France.
[2]British Antarctic Survey, Natural Environment Research Council, Cambridge, UK.

Corresponding author: S. Preunkert, CNRS/UJF–Grenoble 1, Laboratoire de Glaciologie et Géophysique de l'Environnement, UMR 5183, Grenoble, FR-38041, France. (preunkert@lgge.obs.ujf-grenoble.fr)

2169-897X/13/10.1002/2013JD019864

[*König-Langlo et al*., 1998], the difference between the two data sets remains difficult to explain. Furthermore, discussions on the HCHO budget at the two sites led to rather different conclusions. For instance, whereas both studies pointed out that observations cannot be explained by the methane chemistry alone, a minor role of the halogen chemistry is concluded for NM but not for HA, and the snow emission required to explain observations differ from 0.9×10^{13} molecule m^{-2} s^{-1} at HA to 2.5×10^{13} molecule m^{-2} s^{-1} at NM. Since HCHO is a major source of HO_2 radicals in these remote regions [*Bloss et al*., 2007], it is intimately linked to the oxidative capacity of these atmospheres. There is thus a need to better document typical concentrations and to quantify the respective contribution of the gas-phase chemistry and of its various components versus snow emissions in these coastal Antarctic regions.

[5] With this aim, the study of HCHO was initiated at the coastal East Antarctic site of Dumont d'Urville (DDU). Following two pilot studies conducted in November–December 2005 and 2006, HCHO measurements were carried out quasi continuously from 6 January 2009 to 20 January 2010 and again in January–February 2011. Working conditions applied to the analyzers commercialized by the Aerolaser Company were optimized to reach reliable data for mixing ratios as low as a few tens of parts per trillion by volume (pptv), as encountered in winter at this site. Given the absence of a clean air sector at the site of DDU, data were scrutinized with respect to local emissions. Using 0-D and 2-D calculations, the importance of gas-phase photochemical sources and sinks, snow emission, dry deposition, and long-range transport is assessed. Finally, this first year-round record of HCHO gained at the East Antarctic coast is compared to those already available at the West Antarctic coast, enabling a more comprehensive conclusion on the HCHO budget at coastal Antarctica (West and East) to be drawn.

2. Experimental

2.1. Principle

[6] Atmospheric HCHO measurements were performed using two commercial Aerolaser analyzers (model AL-4021) hereafter denoted SN50 and SN39. The technique, a continuous liquid fluorimetry, has been described in detail elsewhere [*Dasgupta et al*., 1988]. Briefly, gaseous HCHO is scrubbed into a diluted sulfuric acid solution in a stripping coil thermostated at +10°C. Then a fluorescent compound, the diacetyl-1,4-dihydrolutidine (DDL), is quantitatively produced at +70°C by the Hantzsch reaction of HCHO with pentane-2,4-dione and ammonia in the liquid phase. Exciting the DDL at 412 nm with an electroluminescent diode and monitoring its fluorescence signal at 510 nm ensures the quantification of HCHO. Liquid reagents were prepared from analytical grade chemicals (Merck) and ultrapure water (18 MOhm, TOC < 1 ppb, Elga Labwater) following the composition given by *Nash* [1953]. After preparation, reagents were purged with He for 10 min and then maintained at +4°C during their subsequent use. In general, reagents were prepared in sufficient quantity to allow measurements to be run over 6 successive days.

[7] To prevent large particles (sea salt, penguin down, and drifting snow) reaching the analyzer inlet, an inertial separator was set up. To do so, air from outside was sucked through a glass venturi tube at a flow rate of 20 L min^{-1}. The HCHO air was sampled in the tube at a flow rate of 2 L min^{-1} perpendicularly to the main air stream. The sampling line was a 2 m long polytetrafluoroethylene tube (0.6 cm). Losses on the tube were found to be less than 5% [*Pépy*, 2011]. Liquid flow rate was measured at the beginning of each run of 6 days with a 200 µL gauged capillary. Depending on the state of the peristaltic pump tubing, which was renewed regularly, the liquid flow was found to fluctuate between 0.38 and 0.43 mL min^{-1}. Under these conditions, the Aerolaser company assures a stripping efficiency higher than 99%, which was confirmed by our calibration experiments (see section 2.2).

[8] Zero air was produced by pumping ambient air through an internal zero trap packed with Hopkalit catalyst. Gas-phase calibrations were done with a gas-phase standard provided by an internal temperature-controlled permeation source (paraformaldehyde, KIN-TEK wafer permeation) through which zero air passed continuously at a flow rate of 100 mL min^{-1}. Raw data (in volts) were monitored continuously with a time resolution of 30 s. Since the zero level and the sensitivity of the system were found to vary over time, zero and gas standard measurements were done regularly (see below) and linearly interpolated to derive HCHO levels. The measurement of a zero and of an internal standard signal takes 25 min each. Detection limits (taken as twice the standard deviation of zero measurements) of 30 pptv (SN50) and 45 pptv (SN39) were determined during zero measurement periods made with 30 s integration time, similar to the value specified by Aerolaser (50 pptv).

[9] During HCHO pilot studies done in 2005 and 2006 at DDU, it quickly turned out that the temperature stabilization set up by Aerolaser in the AL-4021 models purchased before 2008 (heating of the internal source and reactor, cooling of the stripper unit) was not sufficient for our low-level measurements and that changes of the ambient laboratory temperature (up to 15°C from day to night) can induce measurement errors up to a few hundreds of pptv. To overcome this effect, zero determinations and gas standard calibrations were made every 2 h and 12 h, respectively. This was also done during the 2009 campaign even though changes in the laboratory temperature were minimized during this campaign. More details on this temperature effect are reported in Appendix A1.

[10] Aerolaser assigned several potential HCHO interferences for the AL-4021 devices, which were initially equipped with a Hg lamp. These interferences can be neglected for the very remote Antarctic, except the one with ozone for which Aerolaser indicates a positive interference of up to 200 pptv of HCHO at 100 ppbv of O_3. This interference is related to secondary emission peaks of the Hg lamp (between 200 and 600 nm), which are able to excite molecules like O_3 in spite of the use of a filter. The existence of this potential interference was confirmed by the intercomparison study of different HCHO analyzers made by *Wisthaler et al*. [2008]. Since our analyzers are equipped with electroluminescent diodes, which deliver a unique emission peak at 412 nm (half width of 10 nm), no ozone interference is expected. This absence of significant interference can be easily verified by examining our winter data when O_3 values are high and HCHO values are low. Since the Hopkalit trap used to quantify the zeroing signal also removes O_3 from the air stream, a positive O_3 interference

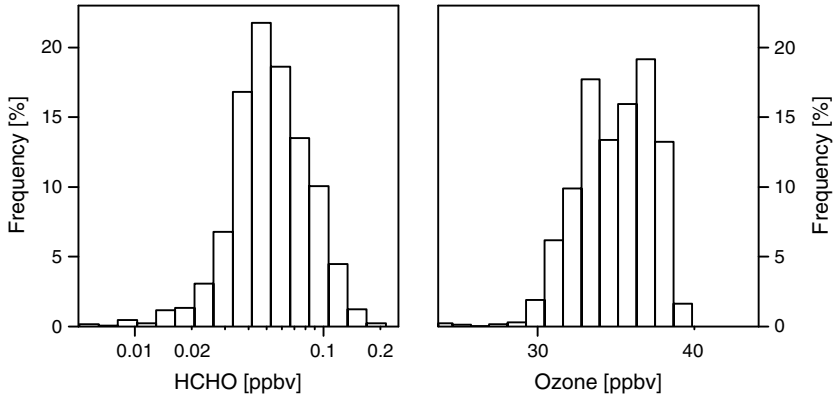

Figure 1. Frequency distribution of 1 h averaged mixing ratios of HCHO and O_3 observed between 1 May and 30 September 2009 at DDU.

will lead to a systematic overestimate of HCHO mixing ratios. The distribution of hourly mean winter values (Figure 1) shows almost no HCHO values lower than 10 pptv, whereas O_3 mainly range between 30 and 40 ppbv. Thus, if it exists, the ozone interference would be less than 10 pptv of HCHO for 35 ppbv of O_3, which is almost 6 times lower than the maximum value proposed by Aerolaser for the mercury lamp equipped models. We therefore conclude that by using an electroluminescent diode in an AL-4021, the HCHO interference with respect to ozone is either eliminated or becomes effectively insignificant.

2.2. Calibrations and Reproducibility of the Two AL-4021 Devices

[11] On-site calibrations were achieved at DDU by comparing the gas-phase standard signal produced by the internal wafers of the AL-4021 analyzers to that of a liquid standard ($20\,\mu g\,L^{-1}$) freshly prepared by diluting a certified stock solution of $0.3\,g\,L^{-1}$ (purchased from the University of Wuppertal, Germany) in the scrubbing liquid in use during the respective day. In addition to possible changes over time of the liquid stock solution, this calibration also accounts for potential losses in the stripping coil (which would result in a collection efficiency lower than unity). After fieldwork was completed, the analyzers were calibrated again at the Laboratoire de Glaciologie et Geophysique de l'Environnement (LGGE) laboratory using two other methods, in line with *Salmon et al*. [2008].

[12] First, a gas-phase calibration was done in which HCHO gas standards were introduced in the analyzer through the sampling line used in the field. Gas standards were provided by a gas calibrator (KIN-TEK, model 491 M) equipped with a certified HCHO source and supplied with air from a pure air generator (Ecophysics, PAG003), which had a Hopkalit trap mounted in series. The signals from different HCHO standards delivered by the calibrator were then compared with the signal from the internal gas standard. This calibration is independent of the liquid standard used in the field but accounts for potential losses in the sampling line and the stripping coil.

[13] Second, a liquid-phase calibration was done in which the internal HCHO gas standard was flowed through two liquid bubblers in series, each filled with stripping solution of the HCHO monitor (i.e., diluted sulfuric acid) (calculated stripping efficiency of 92%). The liquid of each bubbler was then analyzed for HCHO in the liquid mode. This calibration type is therefore independent of potential losses in the stripping coil and the sampling line of the monitor and accounts only for potential errors of the liquid standard used in the field.

[14] The good agreement obtained from the field calibrations and the LGGE liquid calibration (see Table 1) confirms that any losses in the stripping coil are insignificant. The very good agreement between these two methods and the LGGE gas calibration confirms that losses in the sampling line are very small and suggests that the standard liquid solution used in the field had not changed significantly over time. On the basis of these results we have therefore assumed that the internal gas sources of the AL-4021 emit a constant HCHO rate over time, $9.3 \pm 1.4\,ng\,min^{-1}$ for SN50 and $9.9 \pm 1.5\,ng\,min^{-1}$ for SN39 (Table 1).

[15] The SN39 and SN50 analyzers were compared by running them together at the "iono" site (see section 3.2) over 4 days (Figure 2). A Fisher test (N = 580) on 10 min means showed that the mixing ratios derived from the two analyzers are equal at the 95% of confidence interval. Therefore, when running the two analyzers simultaneously at different places (see section 3.2), the two records can be directly compared. The observed signal noise in Figure 2a, which is of electronic origin (D. Haaks, personal communication, 2005), corresponds to a detection limit of 30–45 pptv. The standard deviation of the difference between the two records (hourly averaged values), however, does not exceed 10 pptv

Table 1. Internal Gas Standard Permeation Rates of the Two AL4021 Analyzers (SN39 and SN50) Derived From Three Different Calibration Methods (See Section 2.2)[a]

	Permeation Rates ($ng\,min^{-1}$)	
	SN39	SN50
Field calibration (DDU) (N)	11.27 ± 1.2 (22)	8.89 ± 1.1 (58)
Liquid calibration (LGGE)	10.52 ± 1.1	-
Gas calibration (LGGE)	9.9 ± 1.5	9.3 ± 1.4

[a]The error attributed to the LGGE liquid calibration (10%) is deduced from the observed standard deviation of the N field calibrations. The gas calibration error (15%) is due to uncertainties of the KIN-TEK wafer flow and its HCHO source.

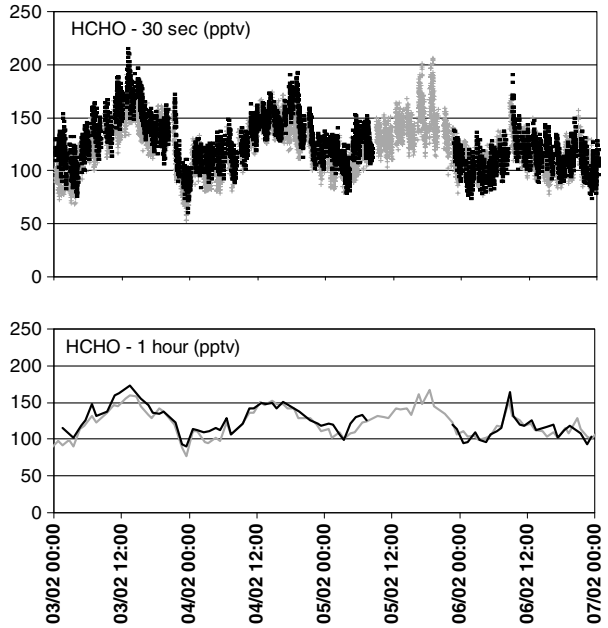

Figure 2. Comparison of HCHO mixing ratios obtained with the SN 39 (grey) and SN50 (black) AL-4021 analyzers at DDU in February 2011 when sampling the same outside air. (top) Raw data recorded with a time interval of 30 s and (bottom) hourly averaged values.

(Figure 2), and variations as low as 10–20 pptv at the scale of a few hours are well detected by the two analyzers.

3. Meteorology and Environment at the DDU Site

3.1. Meteorological Conditions

[16] The DDU station (66°40′S, 140°01′E) is situated on a small island (0.3 km^2) of the Pointe Geology archipelago, located 1 km offshore from the east coast of the Antarctic continent (Figure 3a). The climatology of this coastal site has been described elsewhere [*König-Langlo et al.*, 1998]. In brief, the climate is characterized by two typical situations with either strong katabatic winds coming down from the ice cap situated south of DDU, or zonal easterly winds, appearing with the arrival of low-pressure systems from northern latitudes. As a consequence, the prevailing surface wind direction lies between 120°E (easterly wind) and 160° E (katabatic flow) (see Figure 3). The DDU site thus experiences either air masses coming from inland Antarctica, purely marine air masses, or continental/marine mixed air masses. In contrast to the situation in winter, in summer the katabatic wind strongly decreases or even ceases entirely as temperature rises over midday. Due to this anabatic phenomenon, an apparent "sea breeze" is sometimes observed with local wind direction changing from 120°E–160°E to north. These particular conditions may allow air masses polluted by station activities to reach the sampling sites (Figure 3b).

[17] In order to characterize the origin of air masses reaching the site, backward trajectories were computed using the Hybrid Single-Particle Lagrangian Integrated Trajectory model (R. R. Draxler and G. D. Rolph, NOAA Air Resources Laboratory, Silver Spring, Maryland, 2003, available at http://www.arl.noaa.gov/ready/hysplit4.html). Meteorological data from Global Data Assimilation Process (available at ftp://arlftp.arlhq.noaa.gov/pub/archives/gdas1) were used as input, and the model was run every 6 h in backward mode for 5 days for three different altitudes (0, 250, and 500 m). For each backward trajectory the fractions of air mass residence times over the Antarctic continent (i.e., latitudes > 70°S) and over the open sea (latitudes < 67°S) were calculated. According to that, on average over 1 year, 50 to 70% of air masses advected to DDU are of continental origin while only 10 to 25% are of oceanic origin.

3.2. Local Contamination and Data Reduction

[18] In 2009, year-round HCHO measurements were performed at the sampling site of "labo 3" (see Figure 3b).

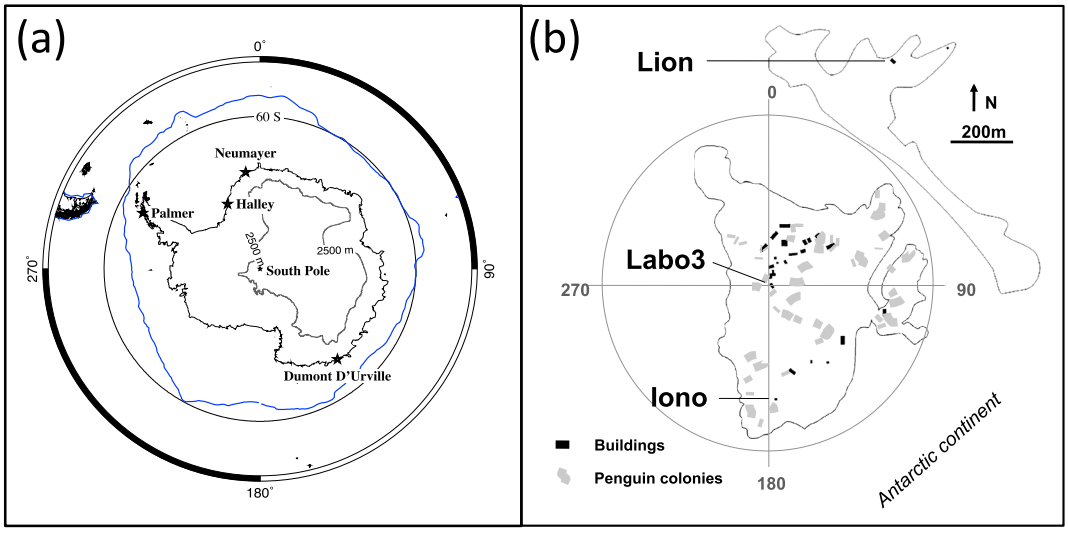

Figure 3. (a) Map of Antarctica showing the locations of Neumayer, Halley, and Dumont D'Urville stations. The blue line refers to the mean location of the sea ice edge in August over the period 1981–2012 (NOAA_OI_SST_V2 data provided by the NOAA/OAR/ESRL PSD, Boulder, Colorado, USA, http://www.esrl.noaa.gov/psd). (b) Map of the Dumont d'Urville station showing the location of the HCHO sampling sites (lion, labo 3, and iono), as well as buildings and penguin colonies.

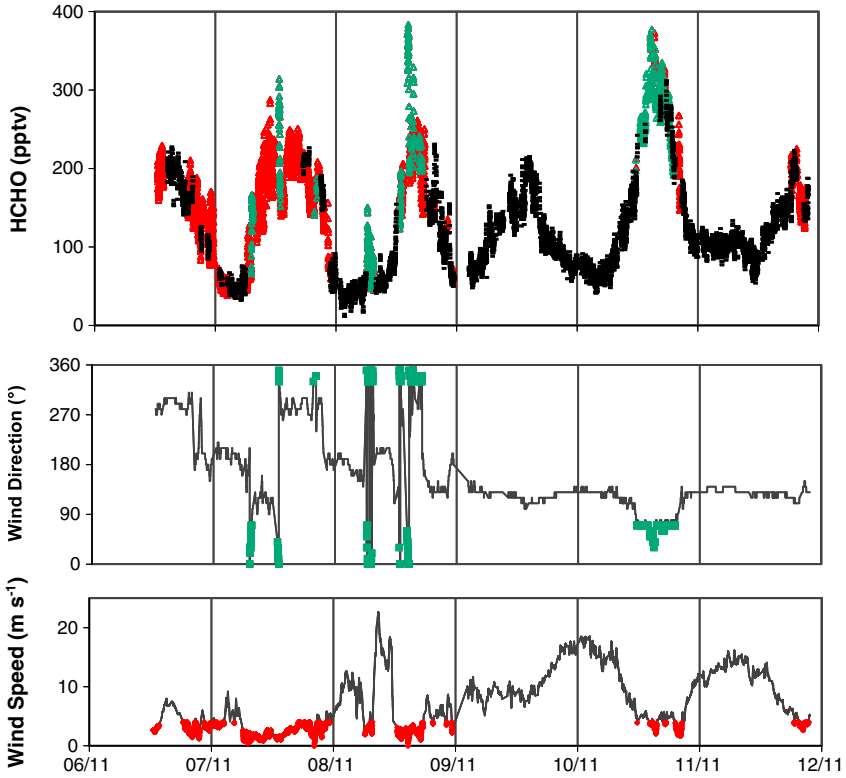

Figure 4. HCHO mixing ratios (30 s) along with wind conditions observed at labo 3 in November 2009. Red triangles refer to low wind speed ($< 4\,m\,s^{-1}$), green triangles to local wind blowing from the main station sector (from 30°W to 70°E, see Figure 3b), and black dots to remaining data.

During the pilot study conducted in 2005 at labo 3, a few sudden enhancements of HCHO mixing ratios (up to 500 pptv within a few minutes) were observed. They were found to originate from indoor contamination when doors or windows of the field laboratory were occasionally left open or when a vehicle approached less than 30 m upwind of the sampling line. Precautions were therefore taken during the 2009–2010 study to minimize such sporadic perturbations that anyway can be easily identified and discarded from the data set.

[19] In addition to vehicular exhausts, station activities also include stationary and quasi-permanent combustion sources of which the effect on the HCHO record at labo 3 is illustrated in Figure 4. When the local wind blew from the main combustion points of the station located between 30°W and 70°E (Figure 3b), systematic enhancements of the HCHO level by 100–150 pptv were detected within a few tens of minutes (e.g., 8 November in the morning and in early afternoon, Figure 4). Furthermore, under low wind speed conditions (less than $4\,m\,s^{-1}$) the HCHO record became noisier (see the case of 7 November in Figure 4) and sporadic enhancements were sometimes detected. To assess this impact of station activities on the HCHO record at labo 3, simultaneous measurements were carried out in summer 2009/2010 at labo 3 and at two other places on the archipelago (iono and lion sites, see Figure 3b) characterized by different clean-air sectors with respect to station activities. Combustion from the station was found to impact HCHO hourly means at labo 3, iono, and lion (up to 150 pptv) under low wind speed conditions and when the wind blew directly from the station sector. Interestingly, during this intersite comparison, another local contamination source was found to impact labo 3 and iono sites under low wind speed conditions ($< 4\,m\,s^{-1}$) and wind directions different to the station sector (i.e., from 70°E to 110°E at labo 3). Enhancements of up to 200 pptv with respect to hourly HCHO means at labo 3 were attributed to this source in 2009/2010. During the 2010/2011 summer season, additional investigations revealed that ornithogenic soils emit numerous volatile organic compounds including HCHO [*Legrand et al*., 2012] and represent another local source of contamination at DDU.

[20] To discard the impact of these two local sources (combustion and penguin emissions) from the data set, a criteria based on local meteorological parameters was used to filter the raw (30 s) data. Data obtained under low wind speed conditions ($< 4\,m\,s^{-1}$) and/or when the wind was blowing from 30°W to 110°E were discarded from the data set. The year-round HCHO mixing ratios obtained at labo 3 in 2009 with raw and filtered data are presented in Figure 5. Note that no significant difference was observed when discarding data with wind speeds lower than $4\,m\,s^{-1}$ and $8\,m\,s^{-1}$ (not shown). In this way, around 40% of data were discarded (29% corresponding to wind speed lower than $4\,m\,s^{-1}$ and 17% to wind blowing from 30°W to 110°E). The highest differences between raw and filtered data are observed from mid-November to mid-December (Figure 5). During this period of the year, fine weather conditions often take place with a general decrease of wind speed at midday. In addition, it is generally at that time that temperatures become close to zero leading to the onset of snow melting at DDU. As discussed by *Legrand et al*. [2012], these wet and mild

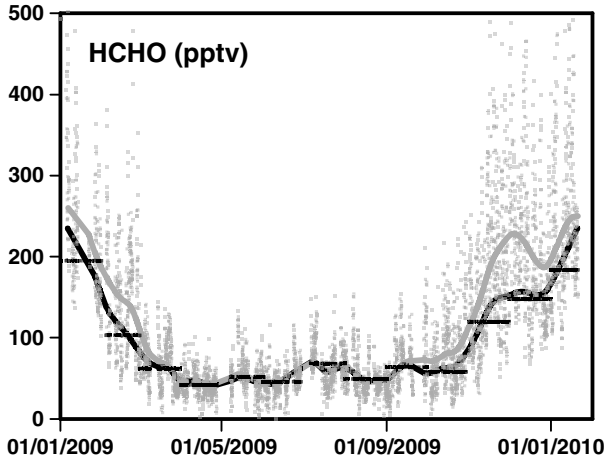

Figure 5. Year-round HCHO record obtained at DDU. Grey dots refer to hourly mean values. Thick lines refer to robust-spline smoothing [*Bloomfeld and Steiger*, 1983] applied to hourly mean values (grey line), and to hourly mean filtered values (black line). The filtered spline and the corresponding monthly means (black horizontal lines) were derived by discarding data which were observed when wind was blowing from 30°W to 110°E or when wind speeds were lower than 4 m s^{-1} (see section 3.2).

weather conditions enhance the bacterial decomposition of guano and the subsequent release of volatile organic compounds to the atmosphere.

[21] Considering zeroing and calibration times, breaks of measurements due to maintenance of the AL-4021 or adverse weather conditions (i.e., snowstorms), the HCHO data set covers around 50% of the total time. This percentage is reduced to around 30% after the filtering procedure. As seen in section 3.1, whatever the season around 60% of air masses advected to DDU were of continental origin against 15% of marine origin. Over the 27% of time for which contamination-free data were available, 60% of data corresponded to continental air and 18% to marine air in summer (70% and 15% in winter, respectively). Thus, no systematic bias was introduced by the breaks in sampling and the filtering procedure.

[22] A well-marked seasonal cycle is observed in 2009 with a winter minimum of 55 pptv and a summer maximum of 200 pptv. Data gained in 2005 and 2006 are limited to November and December months for which monthly mean raw data can be compared to those obtained in 2009. In November, the 175 pptv (unfiltered data) observed in 2009 are comparable to the 150 pptv observed over 19 days in 2005 and 190 pptv over 18 days in 2006. The same consistency can be observed for December with 215 pptv in 2009 against 250 pptv in 2005 (over 17 days) and 182 pptv in 2006 (over 20 days). Finally, for January, the 195 pptv (filtered data) observed in 2009 are also consistent with the 175 pptv observed in 2011 (filtered data).

4. Contribution of Photochemical Productions Versus Snow Emissions to the HCHO Atmospheric Budget at DDU

[23] In the following we discuss HCHO sources and sinks that govern the seasonal HCHO budget at DDU. The importance of local gas-phase photochemical productions and snow emissions as well as long-range transport from lower latitudes are investigated. In addition to the main photochemical sinks (photolysis and reaction with OH) the role of dry deposition is also considered. A 0-D photochemical model is first used to identify the major gas-phase processes that drive the net HCHO production in this region. The model considers CH_4 oxidation as well as the oxidation of other potential precursors such as dimethyl sulfide (DMS) or ethene (C_2H_4), the photolytic destruction of HCHO, and its oxidation by OH. The influence of halogen chemistry on sources and sinks was also examined. The 29 gas-phase reactions included in the model are reported in Table 2 together with their kinetic rates. Since DDU is not located on the snowpack, a 2-D simulation tool (see Appendix B1) was then developed to evaluate the role of inland snow emissions versus gas-phase photochemistry.

4.1. Gas-Phase Photochemical Sources and Sinks of HCHO at DDU

4.1.1. Input Parameters

[24] Summertime OH measurements at coastal West Antarctic sites showed 24 h means of 1×10^5 radicals cm^{-3} at Palmer [*Jefferson et al*., 1998] and 4×10^5 radicals cm^{-3} at HA [*Bloss et al*., 2007]. These values are close to those simulated by global chemistry-transport models such as IMAGES (Intermediate Model of Global Evolution of Species), which predicts OH levels of 2×10^5 radicals cm^{-3} at DDU [*Müller and Brasseur*, 1995]. These simulations, however, do not consider the strong photochemistry induced by the photodenitrification of snow taking place over the Antarctic plateau, as first reported by *Davis et al*. [2001] for the South Pole. The resulting high levels of NO_x there result in an efficient ozone photochemical production [*Chen et al*., 2004] and permit OH levels to reach 2.5×10^6 radicals cm^{-3} [*Mauldin et al*., 2004]. An impact of this very oxidizing canopy at the Antarctic coast is suspected, particularly in East Antarctica where, as discussed by *Legrand et al*. [2009], the katabatic flow frequently brings air masses from the East Antarctic plateau toward DDU. Indeed, the 2004–2008 year-round ozone record indicates a significant influence of the inland oxidizing canopy from mid-November to mid-February at DDU [*Legrand et al*., 2009].

[25] Measurements of OH and RO_2 (HO_2 plus organic peroxy radicals) were conducted from 26 December 2010 to 14 January 2011 (hereafter denoted January 2011) at DDU in air masses of quasi-pure continental origin [*Kukui et al*., 2012]. Compared to measurements carried out at the West Antarctic coast, relatively high concentrations were indeed found with 24 h average values of 2.1×10^6 and 3.3×10^8 radicals cm^{-3} for OH and RO_2, respectively. On the basis of steady state calculations, *Kukui et al*. [2012] showed that the observed OH levels at DDU could be explained simply by assuming some RO_2 to OH conversion mechanism equivalent to the presence of NO in the range of 10 to 50 pptv (30 pptv on average). Note that such a NO level, that largely exceeds those observed at Palmer (1 to 5 pptv) [*Jefferson et al*., 1998], was later confirmed by *Grilli et al*. [2013] who estimated a 24 h average NO level of 13 pptv from NO_2 measurements made in January 2012 at DDU. OH concentrations measured by *Kukui et al*. [2012] in January 2011 were scaled for January, February, November, and December 2009 by considering the observed

Table 2. Gas-Phase Reactions Included in the Photochemical 0-D Model[a]

N°	Reactions	Kinetic Rates	References
	Methane Oxidation		
1	$CH_4 + OH + O_2 \rightarrow CH_3O_2 + H_2O$	$2.45 \times 10^{-12} \exp[-1775/T]$	b
2	$CH_3O_2 + NO \rightarrow CH_3O + NO_2$	$2.30 \times 10^{-12} \exp[360/T]$	c
3	$CH_3O + O_2 \rightarrow HCHO + HO_2$	$7.20 \times 10^{-14} \exp[-1080/T]$	c
4	$CH_3O_2 + CH_3O_2 \rightarrow 2\ CH_3O + O_2$	$(7.40 \times 10^{-13} \exp[-520/T] - 1.03 \times 10^{-13} \exp[800/T])\ 0.35$	c
5	$CH_3O_2 + CH_3O_2 \rightarrow CH_3OH + HCHO + O_2$	$(1.03 \times 10^{-13} \exp[800/T])\ 0.65$	c
6	$CH_3O_2 + HO_2 \rightarrow CH_3OOH + O_2$	$3.80 \times 10^{-13} \exp[780/T]$	c
7	$CH_3OOH + OH \rightarrow HCHO + HO + H_2O$	$(2.93 \times 10^{-12} \exp[190/T])\ 0.35$	c
8	$CH_3OOH + OH \rightarrow CH_3O_2 + H_2O$	$(1.78 \times 10^{-12} \exp[220/T])\ 0.65$	c
9	$HCHO + OH \rightarrow H_2O + HCO$	$5.40 \times 10^{-12} \exp[135/T]$	c
10	$CH_3OOH \rightarrow CH_3O + OH$ ($\lambda < 645$ nm)	J_{MHP}	
11	$HCHO \rightarrow H_2 + CO$ ($\lambda < 337$ nm)	$J_{HCHO\text{-}mol}$	
12	$HCHO \rightarrow H + HCO$ ($\lambda < 360$ nm)	$J_{HCHO\text{-}rad}$	
	Ethene Oxidation		
13	$C_2H_4 + OH \rightarrow HOC_2H_4O_2$	$A = 1 \times 10^{-28}\ (300/T)\ 8.8\ [M]\ B = A / 8.8 \times 10^{-12}$ $C = 1 / (1 + (\log(B)\ \log(B))\ k = (A / (1 + B))\ 0.6^C$	d
14	$C_2H_4 + O_3 \rightarrow HCHO + \text{products}$	$9.10 \times 10^{-15} \exp[-2580/T]$	e
15	$HOC_2H_4O_2 + NO \rightarrow 0.2\ HOCH_2CHO + HO_2 + NO_2 + 1.6\ HCHO$	9.00×10^{-12}	d
16	$HOCH_2CHO + OH \rightarrow 0.8\ HOCH_2C(O)O_2 + 0.2\ HOC_2OH$	1.10×10^{-11}	d
17	$HOCH_2C(O)O_2 + NO \rightarrow HCHO + H_2O_2 + CO_2 + NO_2$	2.00×10^{-11}	d
	DMS Oxidation		
18	$CH_3SCH_3 + OH \rightarrow CH_3SCH_2 + H_2O$	$(1.13 \times 10^{-11} \exp[-253/T])\ 0.20$	e
19	$CH_3SCH_2 + O_2 \rightarrow CH_3SCH_2OO$	5.70×10^{-12}	e
20	$CH_3SCH_2OO + NO \rightarrow HCHO + CH_3S + NO_2$	$4.90 \times 10^{-12} \exp[260/T]$	e
21	$CH_3SCH_2OO + NO_2 + M \rightarrow CH_3SCH_2ONO_2 + M$	$4.90 \times 10^{-12} \exp[260/T]$	e
22	$CH_3SCH2OO + HO_2 \rightarrow CH_3SCH_2OOH + O_2$	1.50×10^{-12}	f
23	$CH_3SCH_2OO + CH_3SCH_2OO \rightarrow 2\ HCHO + 2\ CH_3S + O_2$	1.00×10^{-11}	e
	Reactions With Halogens		
24	$Br + HCHO \rightarrow HBr + HCO$	$2.7 \times 10^{-12} \exp[-580/T]$	g
25	$BrO + CH_3O_2 \rightarrow CH_2O_2 + HOBr$	5.70×10^{-12}	h
26	$IO + CH_3O_2 \rightarrow ?$ (excluding HCHO)	2.00×10^{-12}	i
27	$BrO + HCHO \rightarrow HOBr + HCO$	1.50×10^{-14}	j
28	$Cl + HCHO \rightarrow HCl + HCO$	$8.1 \times 10^{-11} \exp[-34/T]$	c
29	$Cl + CH_4 + O_2 \rightarrow HCl + CH_3O_2$	$6.6 \times 10^{-12} \exp[-1240/T]$	c

[a]Kinetic rates are given in cm^3 $molecule^{-1}$ s^{-1}. The estimations of the photolysis rates for January and June 2009 are given in Table 3.
[b][*DeMore et al*., 1997].
[c][*Atkinson et al*., 2006].
[d][*Ervens et al*., 2004].
[e][*Atkinson et al*., 2004].
[f][*Yin et al*., 1990].
[g][*Atkinson et al*., 2007].
[h][*Atkinson et al*., 2008].
[i][*Salmon et al*., 2008].
[j][*Michalowski et al*., 2000].

change in irradiation with respect to January 2011. NO levels and the HO_2/OH ratio were assumed to be dependent on the OH level following the steady state calculations made by *Kukui et al*. [2012]. On this basis, we estimate a monthly OH mean of 1.5×10^6 radicals cm^{-3} with a corresponding NO mixing ratio of 20 pptv and a HO_2/OH ratio of 84 for January 2009 and 2×10^6 radicals cm^{-3} of OH with 30 pptv of NO and a HO_2/OH ratio of 93 for December 2009. From March to October the photodenitrification of snow on the continent can be neglected and the OH levels predicted by the IMAGE model were considered (see below). As suggested by the ozone record, the influence of the inland oxidizing canopy at DDU was still significant in November and February but less than in December and January. Accordingly, OH values for November and February were calculated as a weighted mean between the scaled OH levels measured by *Kukui et al*. [2012] and the ones simulated by the IMAGE model.

[26] For March to October, calculations were made by assuming NO levels as observed at NM [*Weller et al*., 2002] (i.e., 0.4 pptv in June) and using OH and HO_2 levels simulated by the IMAGE model (i.e., 2.4×10^3 and 1.1×10^6 radicals cm^{-3} in June, respectively).

[27] No direct actinic flux measurements are available at DDU, but as detailed by *Kukui et al*. [2012] photolysis rates can be estimated using the Tropospheric and Visible Ultraviolet radiation model [*Madronich and Flocke*, 1998], and available erythemally weighted UV-B global irradiance (280–320 nm, SolarLight UV-Biometer 501, A. Pazmino, personal communication, 2011), as well as total downwelling solar radiation (SR, 335–2800 nm, Kipp&Zonen 6B Pyranometer) measurements from DDU, respectively. Here we follow the same approach as *Kukui et al*. [2012], except that albedo values were not estimated from UV-B measurements due to a larger calibration uncertainty in 2009. The albedo was assumed to be 0.6 in January 2009 (as calculated by *Kukui et al*., [2012] for January 2011) and 0.85 from March to November, similar to the seasonal mean found at the year-round snow covered HA [*Jones et al*., 2008]. Finally, values for February and December were set to 0.72, which should roughly reflect the typical conditions of seasonal snow coverage at DDU and surrounding sea ice surface.

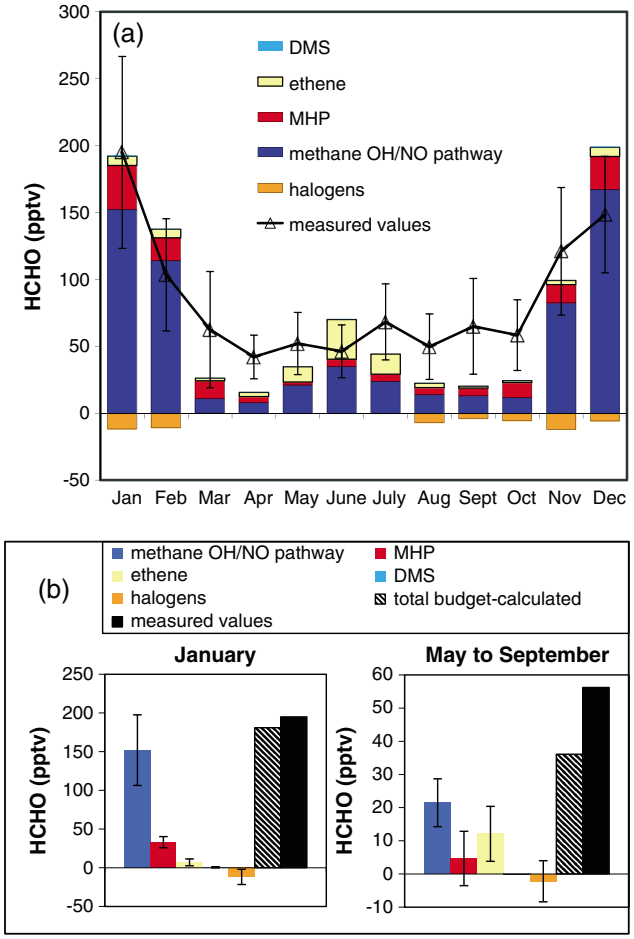

Figure 6. Estimated HCHO contributions from different gas-phase mechanisms and comparison with observations at DDU for the year 2009. Vertical bars refer to (a) monthly variability of observations and (b) calculation uncertainties (see details in sections 4.1.2 and 4.1.3).

[28] Temperature and pressure data provided by the DDU weather station from Météo France and CH_4 data from Syowa Station (69°S) (data available at ftp://ftp.cmdl.noaa.gov/ccg/ch4/flask/event/) were used in our calculations.

4.1.2. Methane Oxidation

[29] In a first step, only CH_4 oxidation by OH together with the two major sinks of HCHO, namely, the photolysis (Table 2, reactions 11 and 12) and the OH reaction (Table 2, reaction 9) are considered in the model. The initial OH attack leads to the formation of the methylperoxy (CH_3O_2) radical which can react with NO to form CH_3O, which is then rapidly converted to HCHO with O_2 (Table 2, reactions 1–3). This reaction sequence is the dominant pathway under high NO conditions, whereas at low NO levels it competes with reactions 4–6 (Table 2).

[30] The corresponding calculated HCHO steady state mixing ratios are reported in Figure 6 on a monthly and seasonal scale. Using input parameter values discussed in section 4.1.1, summer (January, February, November, and December 2009) and winter (May–September 2009) HCHO mixing ratios of 128 pptv and 21 pptv are calculated, respectively.

[31] Methylhydroperoxide (CH_3OOH, hereafter denoted MHP) can form HCHO, CH_3O, or CH_3O_2 (Table 2, reactions 7, 8, and 10). The contribution of MHP to the production of HCHO was examined separately from the CH_4 oxidation pathway with OH and NO (Table 2, reactions 1–6, 9, 11, and 12) since the HCHO year-round study also measured peroxides, H_2O_2, and MHP (see *Preunkert et al.* [2012] for details on working conditions).

[32] With levels of tens to hundreds parts per trillion by volume, MHP was found to be the only organic hydro peroxide present in coastal and inland Antarctic regions [*Riedel et al.*, 2000]. Mean summer (188 pptv in January 2009) and winter (50 pptv from May to September 2009) MHP levels observed at DDU (not shown) are in relatively good agreement with those observed at Neumayer by *Riedel et al.* [2000] (165 pptv and 77 pptv during summer and winter, respectively). The 160 pptv of MHP calculated with our 0-D model for January 2009 conditions are thus consistent with the DDU observations, suggesting that the MHP budget there is mainly driven by CH_4 oxidation. In January 2009 around 33 pptv of HCHO are produced via the MHP breakdown (Figure 6). In winter the MHP breakdown accounts for 5 pptv of HCHO. In this way the MHP pathway accounts for 17% of the total HCHO production from CH_4 oxidation in summer and winter. Note that this contribution remains weaker than that at other remote regions such as the marine boundary layer (36%) [*Wagner et al.*, 2002]. This is probably due to the fact that at DDU air masses mainly arrive from inland Antarctica leading to significant amounts of NO (up to 30 pptv in December, see section 4.1.1) at this coastal Antarctic site, which strengthens the OH/NO methane oxidation pathway (reaction 2) with respect to the HO_2 and MHP pathway (reaction 6).

[33] The uncertainties of the preceding calculations include those linked to the kinetic rates and related to estimates of input parameters like photolysis rates, HO_2/OH ratio, and NO and OH levels. To evaluate the uncertainty linked to the kinetic rates of the methane oxidation reactions, a Monte Carlo study was performed in which all of the rate constants involved (Table 2, reactions 1–9) were modified simultaneously and independently of each other accordingly to their probability distribution. This was done by following the principle described by *Carslaw et al.* [1999] and applied by *Wagner et al.* [2002]. As done in this latter study, respective uncertainty factors were taken for 298 K, and it was assumed that the uncertainty can be approximated by a normal distribution with a variance of one ($\sigma = 1$). One thousand model runs were performed, and the uncertainty on the calculated HCHO mixing ratio related to the kinetic rates was then given by the standard deviation of these 1000 runs, which was found to be close to ± 30 pptv under DDU summer conditions. This value is similar to the one derived by *Wagner et al.* [2002] for the CH_4 oxidation in the marine boundary layer.

[34] A Monte Carlo study was also applied to evaluate uncertainties resulting from input parameter estimations made for the HCHO steady state calculations of January 2009. An uncertainty of 30% was considered for OH levels (see Figures 7a and 7b), corresponding to the daily variability ($\pm$ σ) observed by *Kukui et al.* [2012] in January 2011. Following the interdependence between OH, NO, and the HO_2/OH ratio at DDU under summer conditions (see section 4.1.1), the uncertainties on NO and the HO_2/OH ratio were calculated from the uncertainty in OH. The uncertainty of the derived photolysis rates is estimated to be $\pm 30\%$

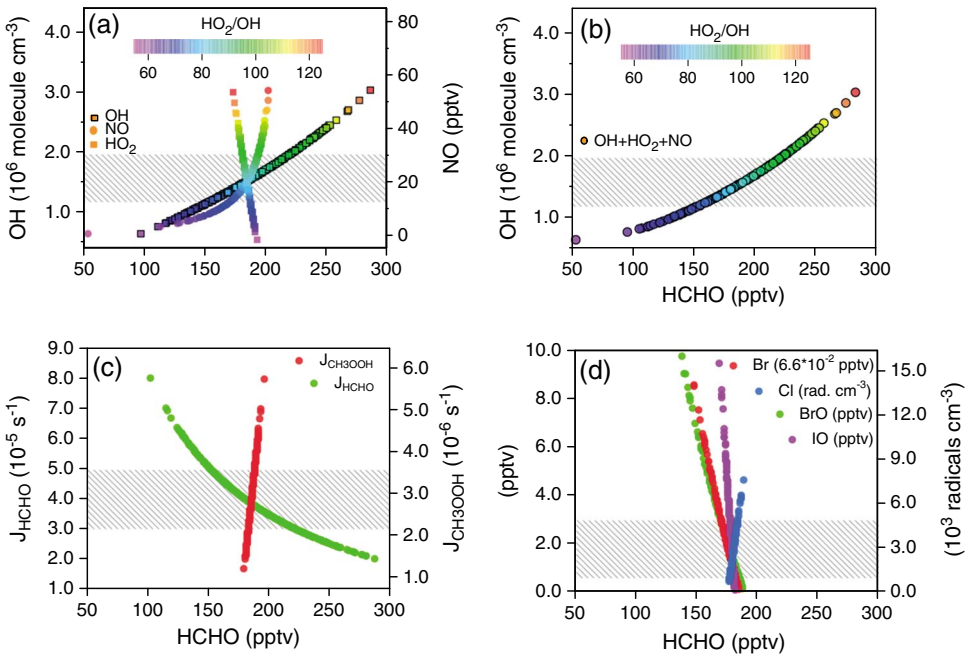

Figure 7. Sensitivity of estimated net photochemical HCHO budget in January 2009. (a–c) Changes of calculated HCHO levels from CH_4 oxidation when OH, NO, or HO_2 values are modified separately (Figure 7a); OH, NO, and HO_2 are changed simultaneously (see section 4.1.1) (Figure 7b), and either J_{HCHO} ($J_{HCHO} = J_{HCHO\text{-}rad} + J_{HCHO\text{-}mol}$) or J_{MHP} inputs are changed (Figure 7c). Note that HO_2 levels can be calculated in Figure 7a by multiplying the OH value by the HO_2/OH ratio. (d) Changes of calculated HCHO levels with respect to different halogen levels (see section 4.1.3). Grey areas refer to the uncertainty ranges of the used input parameters.

[*Kukui et al.*, 2012]. The overall HCHO error derived from this Monte Carlo study reaches ± 45 pptv compared to the 185 pptv of HCHO produced by CH_4 oxidation in January 2009. Figures 7b and 7c show that this total uncertainty is made up of ± 30 pptv from OH, NO, and HO_2 and by ± 30 pptv from photolytic rates. The error of OH thus dominates the errors of NO and HO_2 at the level of OH and NO encountered in summer (Figures 7a and 7b). The main photolytic rate error is due to the HCHO photolysis (Figure 7c). The total uncertainty due to kinetic rates and input parameters on the calculated steady state HCHO mixing ratio in January 2009 reaches ± 55 pptv.

[35] The calculated summer HCHO mean (151 pptv for January, February, November, and December 2009) is very close to the corresponding observations (141 pptv). The monthly difference between observations and simulations is ± 36 pptv (i.e., 25% of the summer mean). For January 2011, for which HCHO as well as OH measurements are available, calculated HCHO overestimates observations by 35 pptv (i.e., 20% of observed values). The differences between observations and calculations are thus similar to the errors in the calculations, suggesting that summer HCHO mixing ratios at DDU can be mainly explained by CH_4 oxidation.

[36] For winter, the uncertainty related to CH_4 oxidation was estimated by assuming NO mixing ratios ranging between 0 and 1 pptv as observed at NM in winter and similar relative uncertainties for the photolytic and kinetic rates as for summer. Since no NO_x emission related to snow nitrate photolysis takes place over the continent in winter, we have assumed that the OH simulations from the IMAGES model are correct and no additional error with respect to the OH levels was considered here. The total uncertainty of the calculated steady state HCHO mixing ratio in winter is around 9 pptv (i.e., 36% of observed values, Figure 6b). The HCHO winter mean estimated from CH_4 oxidation (25 pptv) represents 47% of observed HCHO mixing ratios (56 pptv). Thus, in contrast to summer, other HCHO sources need to be invoked to explain observations in that season.

4.1.3. Contributions From Other Precursors and Role of the Halogen Chemistry

[37] Biogenic emissions of nonmethane hydrocarbons (NMHCs) (light alkenes and DMS) from the Southern Ocean may represent a potential source of HCHO. No ethene data are available for DDU, and in their study limited to 3 days in January 2011, *Legrand et al.* [2012] concluded that propene levels remain below 30 pptv most of the time. At HA, ethene and propene levels close to 17 pptv and 10 pptv were observed throughout the year by *Read et al.* [2007]. With a molar yield of 1.6 (against 1 for propene and lower values for higher alkenes, *Niki et al.* [1981]) and given its relative abundance with respect to heavier alkenes, ethene likely represents the most important alkene precursor of HCHO over the polar ocean. We therefore only consider ethene to evaluate the role of marine alkenes on the HCHO budget (see Table 2, reactions 13–17). Considering 17 pptv of ethene as observed at HA [*Read et al.*, 2007], a HCHO contribution of 7 pptv is calculated for DDU in summer (Figure 6). In contrast to the contribution of CH_4 oxidation, which drops from summer to winter, the contribution of ethene is 2 times higher in winter than in summer (up to 30 pptv in June, Figure 6). This is due to the quasi absence of OH at that time, which favors the reaction of ethene with O_3 whose HCHO yield is higher than that

between ethene and OH. Note, however, that the HCHO winter maximum of 70 pptv calculated for June, essentially driven by the significant HCHO production from ethene, is not confirmed by HCHO measurements.

[38] With a mean DMS summer level of 50 pptv measured at DDU during the HCHO sampling period (data available at http://www-lgge.obs.ujf-grenoble.fr/CESOA/rubrique.php3?id_rubrique=30), a HCHO production of only 0.5 pptv is calculated (Figure 6) using the reaction sequence detailed in Table 2 (reactions 18–23). However, considering a peak value of 1 ppbv of DMS, as occasionally observed at DDU by *Jourdain and Legrand* [2001], 12 pptv of HCHO would be produced; thus, a very sporadic significant contribution of DMS to the HCHO budget cannot be excluded. In winter, both the lower DMS levels (6 pptv) and the weakening of the OH chemistry render the contribution of DMS to the HCHO budget insignificant (less than 0.1 pptv, Figure 6).

[39] Although not fully understood, the influence of halogen chemistry on the HCHO budget has previously been raised [*Salmon et al*., 2008; *Wagner et al*., 2002] and is examined here by considering reactions 24–29 reported in Table 2. Halogen chemistry can represent a net destruction or production of HCHO, depending on the competition between the destruction by BrO, IO, and Br (reactions 24–28) and the production via the reaction of Cl with CH_4 (reaction 29). Spatial and temporal variability of tropospheric BrO columns shows that regions with enhanced tropospheric BrO columns exhibit an excellent correlation with the areas of sea ice, located along the coast line of Antarctica [*Theys et al*., 2011]. As there is less sea ice in the Indian sector (DDU) than in the Atlantic sector (HA), bromine chemistry may play a weaker role at DDU than at HA. Note that this is also confirmed by the occurrence of far less frequent spring Ozone depletion events at DDU than in the Atlantic sector [*Legrand et al*., 2009]. Year-round ground-based measurements of IO and BrO conducted at HA by *Saiz-Lopez et al*. [2007] have shown that both species are present from September to April at mixing ratios close to 3 pptv (maximum of 6 pptv in October). Though these similarities are not fully understood it is likely that (as for BrO) the iodine chemistry would be less important at DDU than at HA. Comparing BrO and IO data observed at HA [*Saiz-Lopez et al*., 2007], and satellite data of total BrO columns between HA and DDU [*Theys et al*., 2011], upper limits for BrO and IO mixing ratios were taken as half of the monthly mean values of HA (i.e., 1.5 pptv) for DDU in January and an upper limit of 3 pptv for spring. Note, however, that even though very limited over time, recent ground-based measurements of IO and BrO conducted in January 2012 at DDU indicated BrO values below 2 pptv over 4 days and IO mixing ratios of 0.04–0.15 pptv over 20 days [*Grilli et al*., 2013], well below our upper estimate of 1.5 pptv. Similar to *Salmon et al*. [2008], a crude estimation of Br levels was achieved from steady state calculations considering the BrO photolysis and the Br reaction with O_3, leading to mixing ratios up to 0.07 pptv in summer. Even though somewhat speculative, we have assumed that, as suggested by *Read et al*. [2007] for HA in spring, 2.3×10^3 radicals cm^{-3} of Cl are present at DDU in summer.

[40] Figure 7d illustrates the influence of the four halogens on the calculated HCHO mixing ratios. It can be seen that a larger presence of Cl would lead to a net increase of HCHO levels, while enhanced IO levels would lead to lower HCHO levels. The strongest impact on HCHO levels is, however, related to BrO and Br, both acting as a sink of HCHO. For example, the doubling of the assumed summer levels of either Cl, IO, Br, or BrO would lead to a HCHO change of +5, −3, −6, or −10 pptv, respectively. Considering conditions assumed for January 2009, a destruction of 12 and 15 pptv of HCHO is calculated for summer in the presence or absence of Cl, respectively. In spite of the large uncertainty on the Cl level, Figure 7d shows that HCHO mixing ratios remain moderately sensitive to this parameter. During winter BrO and IO values were found to be below instrumental detection limits at HA [*Saiz-Lopez et al*., 2007], and we thus neglected halogen chemistry at DDU at least from April to July. Although these calculations are very uncertain, they suggest that the halogen chemistry has a rather weak impact on the HCHO budget at DDU (see Figure 6).

[41] The uncertainties related to NMHC oxidation and halogen chemistry were calculated following the Monte Carlo method described in section 4.1.2 and considering the following uncertainties on the levels of ethene and of the various halogens in summer (and winter): ethene 7–30 pptv (7–30 pptv); IO and BrO 0.7–3 pptv (0.2–1.1 pptv); Br 0.02–0.2 pptv (0.001–0.008 pptv); Cl_{rad} $1.5–3.5 \times 10^3$ radicals cm^{-3} ($3–7.5 \times 10^2$ rad cm^{-3}) (Figure 6b).

4.2. HCHO Snow Emissions in the Vicinity of DDU

[42] HCHO snow emissions from the inland Antarctic region located near DDU were estimated on the basis of snow flux data available in the literature. Experimental and modeling studies of HCHO air/snow exchange provided consistent results in reconstructing HCHO levels in snow and air at Greenland (Summit) and Antarctic (the South Pole) sites. Whereas empirical thermodynamic considerations suggested that site conditions like snow accumulation rates (A) and temperatures (T) mainly govern the intensity of HCHO air/snow exchanges [*Hutterli et al*., 2003], potential emissions due to photolytic degradation of organic matter seem to be limited at inland polar ice sheets sites as Summit [*Hutterli et al*., 1999] and the South Pole (e.g., < 20% at the South Pole [*Hutterli et al*., 2004]). HCHO emissions are generally larger at sites with high snow accumulation rates than at those with low snow accumulation rates where the snowpack can even act as a sink [*Frey et al*., 2005; *Hutterli et al*., 1999, 2004; *Jacobi et al*., 2002]. Furthermore, at a given site, warm temperatures strengthen snow emissions, following the thermodynamic equilibrium between ice and air. *Hutterli et al*. [1999, 2004] measured and estimated summer fluxes at Summit ($A = 20$ g H_2O cm^{-2} yr^{-1} and mean annual T of −30°C) to be $1.4–8.8 \times 10^{12}$ molecule m^{-2} s^{-1} and summer and winter fluxes at the South Pole ($A = 8$ g H_2O cm^{-2} yr^{-1} and mean annual T of −50°C) to be 2×10^{12} molecule m^{-2} s^{-1} and 0.1×10^{12} molecule m^{-2} s^{-1}, respectively. Note that although the preceding model approach does not consider the precise nature of processes governing the HCHO exchange between air and ice recently highlighted by *Barret et al*. [2011], they reflect quite well observations made at polar sites and are thus appropriate for our application.

[43] Considering typical wind speeds and atmospheric HCHO lifetimes against photochemistry (i.e., a few hours in summer and a few weeks in winter), the snow-covered area that may influence the HCHO budget at DDU in summer

Table 3. Estimated Input Parameters for January and June 2009 Used in Photochemical HCHO Calculations (See Section 4.1.1)

Month	T (°C)	P (mbar)	CH_4 (ppbv)	O_3 (ppbv)	OH (rad cm^{-3})	HO_2 (rad cm^{-3})	NO (pptv)	$J_{HCHO\text{-}mol}$ (s^{-1})	$J_{HCHO\text{-}rad}$ (s^{-1})	J_{CH3OOH} (s^{-1})
January	−0.9	986	1730	18	1.51×10^6	1.25×10^8	20	2.5×10^{-5}	1.4×10^{-5}	2.7×10^{-6}
June	−15.3	986	1690	34	2.4×10^3	1.1×10^6	0.5	1.3×10^{-7}	0.7×10^{-7}	1.4×10^{-8}

extends up to 700 km inland from DDU. After a narrow margin region of 20 km where snow does not accumulate in this inland sector, A values remain close to 35 g cm^{-2} yr^{-1} over the first 150 km [*Agosta et al*., 2011] and then steadily decrease to 18 g cm^{-2} yr^{-1} at 500 km from DDU [*Arthern et al*., 2006]. The mean annual air temperature decreases from −10°C near DDU to −25°C and −40°C at 110 km and 500 km from DDU, respectively (see Tables 3 and 4). These conditions are quite similar to those encountered in the Summit region. As a crude estimate, we have therefore assumed a HCHO snow emission in the DDU Antarctic sector of $0.5–1 \times 10^{13}$ molecule m^{-2} s^{-1} in summer and $0.5–1 \times 10^{12}$ molecule m^{-2} s^{-1} during winter (i.e., scaled down on the order of magnitude of the summer to winter HCHO flux ratio observed at the South Pole).

4.3. Relative Contribution of Photochemical Productions and Snow Emissions

4.3.1. Role of Photochemical Productions Versus Snow Emissions in Summer

[44] As discussed in section 4.1.3, the contribution of the DMS oxidation to the HCHO budget remains minor in summer. Therefore, this process was neglected in 2-D simulations of the gas-phase summer photochemistry. Two-dimensional simulations indicate an increase of HCHO mixing ratios from 185 to 210 pptv at DDU in January when a snow emission of

Table 4. Measured HCHO Mixing Ratios, Initial and Updated Input Parameters Used for Photochemical Calculations, Dry Deposition Velocity, Overall Estimated HCHO Mixing Ratios Considering CH_4 Oxidation and Halogen Chemistry, and Their Respective Contributions at HA and DDU[a]

	HA 75°35′S, 26°39′W		DDU 66°40′S, 140°01′E
	Salmon et al. [2008] 3 Jan to 10 Feb 2005	This Study 3 Jan to 10 Feb 2005	This Study January 2009
HCHO: measured (pptv)	127	127	195
OH (rad cm^{-3})	3.9×10^5	3.9×10^5	1.51×10^6
HO_2 (rad cm^{-3})	$53 \times OH$	$53 \times OH$	$84 \times OH$
NO (pptv)	7.3	7.3	20.2
MHP (pptv)	-	191	188
Br (pptv)	0.8	0.45[b]	0.07
BrO (pptv)	2	2	1.4
IO (pptv)	2	2	1.4
Cl_{rad} (rad cm^{-3})	-	2.3×10^3[c]	2.3×10^3
J_{HCHO}[d] (s^{-1})	1.7×10^{-5}	7.0×10^{-5}[e]	3.9×10^{-5}
CH_4 (ppbv)	1720	1720	1730
Deposition velocity (cm s^{-1})	-	(0.4)	(0.4)
HCHO: overall gas-phase photochemical sources and sinks including CH_4 oxidation and halogen chemistry (pptv) (including dry deposition)	40 n.c.	36 (22)	173 (135)
HCHO: CH_4 oxidation including MHP (pptv)	99 (without HP)	45	185
HCHO: halogen chemistry (pptv)	−44 −82	−9	−12
HCHO: attributed to snow emissions (pptv) (including dry deposition)	87	82 (102)	(~45)
Snow emission (molecules m^{-2} s^{-1}) (including dry deposition)	0.88×10^{13}	1.15×10^{13}	
	n.c	(2.5×10^{13})	(2.0×10^{13})
BDL height (m)	100	70	300
Mean annual air temperature (°C)	−19[f]		−10.8[g]
	−20 − −45[g]		−20 − −40[g]
Annual accumulation rate (gH_2O cm^{-2} yr^{-1})	36[h]		0
	5 − 25[i]		10 − 35[i]

[a]Snow emission fluxes (adjusted to fit measurements at HA) and estimated from the literature and the observed daily variation of HCHO in the case of DDU (see section 4.3.1) as well as boundary layer heights, air temperatures, and snow accumulations are reported. Underlined values refer to measurements, others to estimated values. "n.c." denotes "not considered".

[b]Estimated from steady state calculations between BrO photolysis and the $Br + O_3$ reaction. For HA and DDU typical ozone mixing ratios in January of 7 ppbv [*Jones et al*., 2008] and 18 ppbv [*Legrand et al*., 2009] were assumed, respectively.

[c]Data from *Read et al*. [2007].

[d]$J_{HCHO} = J_{HCHO\text{-}rad} + J_{HCHO\text{-}mol}$.

[e]Data from http://badc.nerc.ac.uk/browse/badc/chablis/data.

[f]*König-Langlo et al*. [1998].

[g]Data from THERMAP (*Antarctic Ice Sheet Temperature Data*), available at http://nsidc.org/data/thermap/antarctic_10m_temps/dixon_map.html.

[h]*Limbert* [1963].

[i]*Arthern et al*. [2006] accounting also for the adjacent upwind sectors.

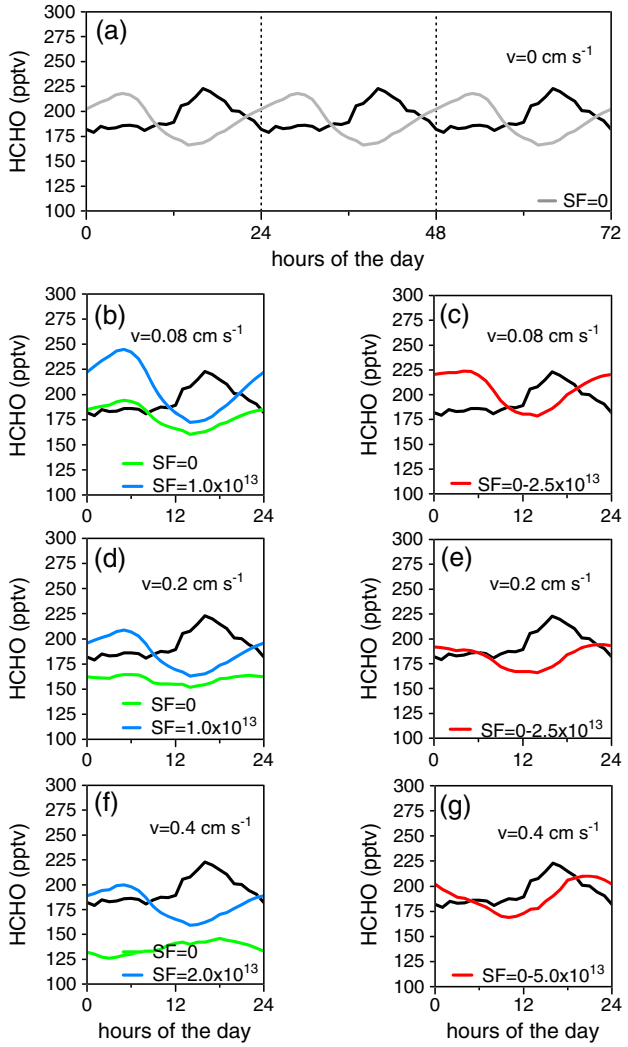

Figure 8. Mean daily HCHO variation observed during summer at DDU (black line) compared to calculations considering (a) photochemical sources and sinks and (b–g) photochemical sources and sinks together with different deposition velocities (v in cm s^{-1}) and snow fluxes (SF in molecule m^{-2} s^{-1}) as discussed in section 4.3.1. Simulations were made using January conditions (see Table 3 and Appendix B1).

1×10^{13} molecule m^{-2} s^{-1} is added without considering HCHO dry deposition. On the other hand, the consideration of dry deposition of HCHO without any snow emission would decrease the calculated mixing ratio. Though the dry deposition velocity of HCHO on snow and ice is poorly known, with proposed values ranging from 0.025 cm s^{-1} [*Riedel*, 2001] to 0.5 cm s^{-1} [*Zhang et al.*, 2003], the calculated mixing ratio in January decreases from 192 pptv to 184 pptv if a dry deposition velocity (v) of 0.08 cm s^{-1} is assumed and to 166 pptv with $v = 0.2$ cm s^{-1} (i.e., the value obtained when applying the dry deposition parameterization detailed in Appendix B1).

[45] The examination of the diurnal HCHO variation can provide further information in terms of sources and sinks of HCHO. Indeed, in addition to diurnal change of photolytic conditions and strength of snow emissions (see below), the dry deposition, which is kept constant (see Appendix B1), may influence the HCHO levels over the course of the day [see *Wagner et al.*, 2001]. At DDU in summer, a HCHO maximum is very often observed in the late afternoon. The DDU site is not surrounded by snow-covered areas in summer and diurnal changes may be related to changes in air mass having been, or not been, in contact with snow-covered surfaces. In summer, the katabatic wind that often blows in the morning bringing air from inland Antarctica sometimes becomes null as temperature rises over midday, resulting in wind blowing from the open ocean in the afternoon. As discussed in section 3.2, these particular conditions may permit air masses polluted by station activities to reach the sampling sites leading to an increased HCHO level in the afternoon. Discarding these particular days and focusing on those during which continental flow was maintained over the entire day, a HCHO maximum can still be detected in the afternoon (Figure 8a).

[46] While under katabatic flow conditions we can observe a mean increase of 40 pptv in the late afternoon, photochemical budget calculations predict a decrease of ~50 pptv from early morning to middle afternoon (see Figure 8a). As seen in Figures 8b and 8d the introduction of dry deposition not only leads to a decrease in averaged daily values but also minimizes the simulated afternoon minimum. When a v value as high as 0.4 cm s^{-1} is applied (average daily HCHO value of 135 pptv, Figure 8f), the simulated diurnal cycle starts to show a maximum in the afternoon. In fact, the net destruction of HCHO at night provided by dry deposition, which is counterbalanced by HCHO production during the day, leads to a HCHO maximum in the afternoon. Considering a variable snow emission source (mean of 1×10^{13} molecule m^{-2} s^{-1} adjusted according to the diurnal temperature cycle of air and snow, see Appendix B1) with v value of 0.2 cm s^{-1} (Figure 8e), calculations simulate a daily cycle, which starts to become similar to observations. However, the simulated maximum is broader and takes place 6 h later compared to observations and the amplitude is of only ~25 pptv. The best agreement with respect to the diurnal cycle and the mean daily HCHO level between calculations and observations is obtained when a variable snow emission source (mean of 2×10^{13} molecule m^{-2} s^{-1} adjusted according to the diurnal temperature cycle of air and snow) and a v value of 0.4 cm s^{-1} is considered (diurnal change close to 40 pptv and daily mean of 190 pptv, Figure 8g). Note that a further increase of the dry deposition velocity together with an increase in snow emissions will not improve the agreement between observations and calculations but result either in an underestimation of the mean daily HCHO level (if the diurnal change is fitted to observations) or in an overestimation of the daily amplitude (if the daily mean is fitted to observations).

[47] As seen in Figure 9 where a snow emission of 2×10^{13} molecule m^{-2} s^{-1} and a v value of 0.4 cm s^{-1} were assumed, it appears that the budget of HCHO in summer at DDU is largely controlled by the gas-phase photochemistry with methane acting as the main precursor, the impact of snow emissions being less significant.

4.3.2. Role of Photochemical Productions Versus Snow Emissions in Winter

[48] The gas-phase photochemical production in winter accounts for around 36 pptv of HCHO (25 pptv from methane and 12 pptv from ethene, Figure 6b). The inclusion of a dry deposition of HCHO without any snow emissions decreases the calculated mixing ratio to 8 (4 pptv) if a deposition velocity of 0.2 (0.4) cm s^{-1}, i.e., similar as estimated for summer

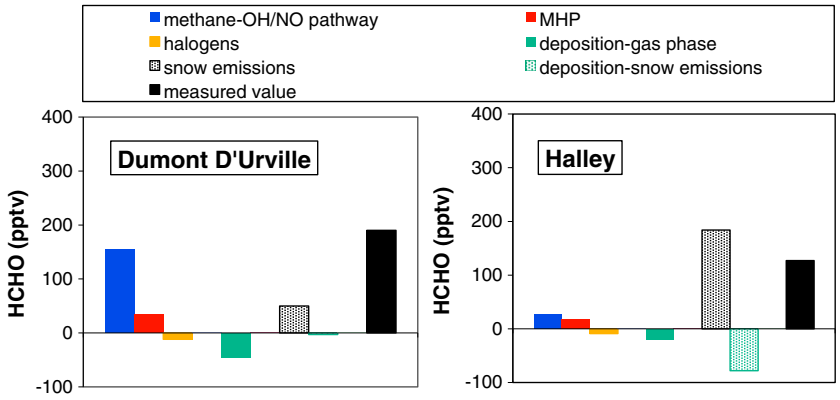

Figure 9. Estimated contributions to HCHO summer (January) mixing ratios at (left) DDU and (right) HA. Calculations consider photochemistry of CH_4 (OH/NO pathway in blue and MHP breakdown in red), halogen chemistry (in orange), and the dry deposition applied to preceding contributions (green). The HCHO contributions from snow emissions and their dry deposition (dotted green and black areas) are also shown. Note that the snow flux was adjusted to fit measurements (black) in the case of HA (with a deposition velocity of 0.4 cm s^{-1} and a BDL height of 70 m) and estimated from the literature and the observed daily variation of HCHO in the case of DDU (see section 4.3.1 and Table 4).

(see Appendix B1), is considered. This stronger effect of dry deposition in winter compared to summer is due to the fact that chemical HCHO sinks (i.e., photolysis and oxidation with OH radicals) are about an order of magnitude slower than the deposition sink in that season. In addition, the boundary layer (BDL) height tends to be shallower in winter (from 100 to 300 m, [*Gallée et al.*, 2012]) than in summer.

[49] Given the weak photochemical activity in winter, the HCHO budget in that season can be examined by considering only HCHO snow emission and dry deposition. Note that since the source and sink terms depend in the same way on the BDL height, the result of calculated mixing ratios becomes independent of the BDL height. Considering the crude winter snow flux estimate ($0.5–1 \times 10^{12}$ molecule m^{-2} s^{-1}) made in section 4.2 for winter conditions over the continent in the vicinity of DDU, 4–8 pptv and 9–18 pptv HCHO are produced from the snowpack assuming deposition velocities of 0.4 and 0.2 cm s^{-1}, respectively. Note that under these winter conditions steady state levels are reached after 3 to 12 days. Considering a contribution of 10 pptv related to long-range transport of HCHO (see below), and as discussed above an upper limit a gas-phase contribution (including dry deposition) of the same order of magnitude, around 30 pptv are expected to be related to snow emissions to reproduce observed HCHO winter mixing ratios at DDU. Assuming similar deposition velocities as estimated for summer, likewise as found for the latter season, 2 to 3 times higher snow fluxes than estimated from literature (i.e., $2–3 \times 10^{12}$ molecule m^{-2} s^{-1}), would be needed to match observations.

[50] Since HCHO losses due to its photolysis and reaction with OH become very inefficient at high southern latitudes in winter, dry deposition processes control the atmospheric HCHO lifetime in that season. Assuming a deposition velocity of 0.4 cm s^{-1} over the ocean [*Wagner et al.*, 2002] and a typical marine BDL height of ~1300 m [*Sciare et al.*, 2000], the HCHO lifetime would reach some 3 to 4 days in winter. Thus, an air mass located at midlatitudes with a typical level of 200 pptv HCHO [*Lowe and Schmidt*, 1983], that was then transported within a few days to the Antarctic coast, should still contribute several tens of pptv of HCHO at DDU in winter. To identify and estimate such an influence of long-range transport from lower latitudes on the HCHO budget at the coastal Antarctic site of DDU, we examine the high-resolution winter record. In Figure 10 we report hourly mean HCHO levels at DDU in midwinter together with air mass residence time fractions derived from back trajectories obtained from HYSPLIT (see details in section 3.1). As seen in Figure 10, during July and August, days characterized by an increase of HCHO levels (up to 100 pptv above the mean winter value of 55 pptv) coincided quite well with arrival of air masses of marine origin at the site. For example, after having encountered air masses of continental origin over more than 6 days at the end of July and beginning of August, an advection of marine air, located 5 days before at 45°S, took place at DDU on 6 August and was followed by an increase in hourly mean HCHO levels up to 150 pptv. Similar marine air advections took place from 8–11 July, 26–28 July 2009, 10–12, and 18–22 August 2009 (Figure 10). Comparison between the average winter level and the one calculated by considering only periods over which air masses were of pure continental origin suggests that on a monthly average, the long-range transport contributed around 10 pptv of HCHO during winter 2009 at DDU.

[51] In conclusion, the weakened photochemistry and a contribution from the long-range transport each account for less than 20% of the observed HCHO making snow emissions the largest source at DDU in winter.

5. Comparison With Data Available at the West Antarctic Coast

[52] Two year-round HCHO records were previously obtained, at NM from March 1997 to January 1998 [*Riedel et al.*, 1999] and at HA from May 2004 to January 2005 [*Salmon et al.*, 2008], two sites located at the coast of West Antarctica (Figure 3a). Large differences appear between these two records with values ranging between 100 and 200 pptv in winter and exceeding 450 pptv in

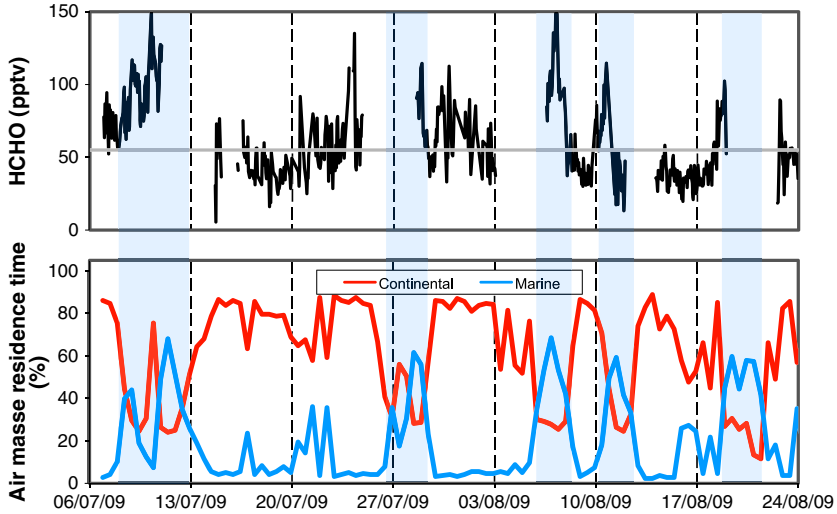

Figure 10. (top) Hourly mean winter HCHO mixing ratios observed at DDU from July to August 2009 (black line) together with the overall mean HCHO winter level of DDU (horizontal grey line). (bottom) Continental (red line) and marine (blue line) residence time fractions of air masses arriving at DDU as deduced from the HYSPLIT model (see section 4.3.2). Blue shaded periods refer to marine air mass arrivals at the site.

summer at NM, against ~ 50 pptv and 130 pptv at HA in winter and summer, respectively.

[53] These differences, that are unexpected for two sites experiencing rather similar conditions, may be related to working conditions applied to the deployed Aerolaser analyzers. As detailed in Appendix A1, it was discovered that the signals of the Aerolaser analyzers are sensitive to ambient temperature changes (from −50 pptv per °C to + 100 pptv per °C depending on the temperature gradient), which may lead to significant biases with respect to the low atmospheric levels encountered in polar region. The 12 h interval of zero measurements applied at NM [*Riedel et al.*, 1999] associated with the fact that (to keep the sampling lines as short a possible) the analyzer was run in the nonthermostated entrance of the Air Chemistry Observatory, where temperatures fluctuated between 13 and 30°C [*Riedel*, 2001], may have therefore induced significant errors. It remains, however, difficult to quantify this effect without checking raw signal and zero values along with the air temperature of the field laboratory. In the following we therefore concentrate discussions on the site of HA and DDU where more frequent zero estimations were made (3 h and 2 h, respectively) to overcome these biases related to lab temperature changes.

[54] Figure 11 compares monthly mean HCHO mixing ratios observed over the course of 1 year at HA and DDU. The two records show a seasonal cycle characterized by winter minima close to 50 pptv. In summer, monthly mean values reach 130 pptv at HA against 185 pptv at DDU in January. The examination of processes controlling the observed levels suggest that at DDU gas-phase photochemistry largely controls the HCHO budget (see section 4.3.1), whereas at HA it accounts for only 15% and a dominant contribution from snow emissions is suspected. Several differences in the assumptions made for the two sites make it, however, difficult to draw a comprehensive conclusion about the budget in coastal Antarctica. Among others, the MHP chemistry as well as the HCHO dry deposition on snow was considered at DDU but not at HA. Furthermore, the discussion conducted in the two studies raise several questions that needed to be addressed. First, steady state calculations suggest that in January 150 pptv of HCHO are related to the OH/NO methane oxidation at DDU (Figure 6), whereas *Salmon et al.* [2008] calculated 99 pptv at HA. Such a difference between the two calculated values is surprisingly small given the 4 times higher OH concentrations observed at DDU (24 h average of 2.1×10^6 radicals cm^{-3} [*Kukui et al.*, 2012]) compared to HA (24 h average of 4×10^5 radicals cm^{-3} [*Bloss et al.*, 2007]). Also unclear is the role of halogen chemistry, with a calculated net sink of 44 to 82 pptv of HCHO at HA [*Salmon et al.*, 2008] against 12 pptv at DDU (section 4.1.3). Second, the consistency of snow emissions proposed by *Salmon et al.* [2008] to match observations at HA cannot be directly compared with our estimate for DDU (sections 4.2 and 4.3.1) since no dry deposition was considered for HA.

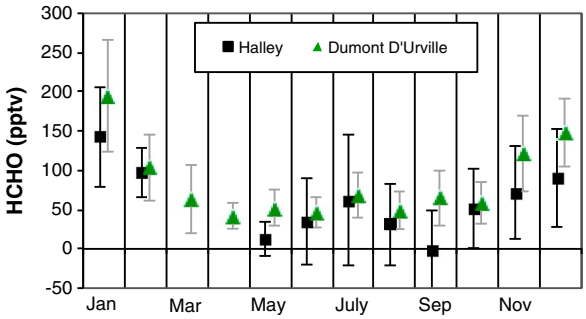

Figure 11. Monthly mean HCHO mixing ratios measured at HA between January 2004 and February 2005 [*Salmon et al.*, 2008] (black squares) and at DDU between January 2009 and January 2010 (this study) (green triangles). Vertical bars refer to standard deviations of 10 min and 1 h data in the case of HA and DDU, respectively.

[55] At both sites HCHO represents the main source of HO_2 radicals in summer (see *Bloss et al*. [2007] for HA and *Kukui et al*. [2012] for DDU). There is therefore a strong need to gain a more comprehensive understanding of the HCHO budget in summer at coastal Antarctica (West and East) where the nature and level of oxidants as well as meteorological conditions are different. With this aim, we compare in the following the importance of gas-phase photochemistry, snow emission, and dry deposition for the two sites under summer conditions.

5.1. Gas-Phase Photochemical Sources and Sinks in Summer

[56] Previous investigations of HCHO photochemical productions and sinks made for conditions encountered at HA by *Salmon et al*. [2008] are compared with those made at DDU in section 4.1. The two studies pointed out that the most important gas-phase processes controlling the HCHO level are, in addition to photochemical losses, related to the HO_x methane oxidation and in the case of HA the halogen chemistry. There are, however, a few important differences in parameters used to derive the respective HCHO contributions between the two studies. For instance, the value of the 24 h averaged HCHO photolysis rate (J_{HCHO}) used in the calculations is lower at HA (1.7×10^{-5} s^{-1}) than at DDU (3.9×10^{-5} s^{-1}, Table 4) which is inconsistent with solar radiation differences between 66°S (DDU) and 75°S (HA). Furthermore, the MHP was not considered by *Salmon et al*. [2008] at HA. Assumptions on Cl and Br levels affect the contribution of halogen chemistry to the HCHO budget. For instance, whereas rather similar IO, BrO, and Cl levels were assumed at HA and DDU, a strong HCHO destruction is calculated at HA compared to DDU. This is a result of the lower HCHO photolysis rate and a higher Br level at HA (0.8 pptv instead of 0.07 pptv at DDU, Table 4).

[57] These inconsistencies required a critical reexamination of the estimations reported in Table 4. These new calculations were performed for January using the 0-D model detailed in section 4.1 and focus on main processes (i.e., reactions related to CH_4 oxidation, major HCHO destruction pathways, and the halogen chemistry). Given the importance of the HCHO photolysis which dominates the other gas-phase sinks (i.e., HCHO reaction with OH and halogens), it is crucial to elucidate the inconsistencies in J_{HCHO} values used in the two studies. It appears that the validated 2-π J_{HCHO} value for HA in January 2005 (available at http://badc.nerc.ac.uk/browse/badc/chablis/data) is about a factor 2 higher than the photolysis value used by *Salmon et al*. [2008]. Accounting also for the upwelling radiation at HA [*Jones et al*., 2008] the HCHO photolysis rate considered for HA amounts to 7×10^{-5} s^{-1}. The reevaluation of the contribution of methane oxidation for HA (45 pptv of HCHO) is half of the initial evaluation (99 pptv) made by *Salmon et al*. [2008] which is due to the use of the updated, ~4 times higher J_{HCHO} value. This decrease is somewhat mollified since a part of it is compensated for the production of HCHO via the HO_2/MHP breakdown pathway that was not considered by *Salmon et al*. [2008] but which makes up 18 of the 45 pptv in our study. The 18 pptv of HCHO produced from the MHP breakdown were calculated here by assuming that the 191 pptv of MHP measured at NM in November 1997 [*Riedel et al*., 2000] are representative for summer at HA, where no measurements are available. Note that the contribution of the MHP breakdown to the total CH_4 oxidation is 2 times more at HA than at DDU due to the higher NO level at DDU.

[58] The role of halogen chemistry was considered at HA by applying the same IO and BrO values as *Salmon et al*. [2008]. The Br atom level estimated by *Salmon et al*. [2008] for Halley (0.8 pptv) was derived from model simulations, which included the equilibrium between BrO photolysis and the reaction of Br with ozone as well as effects of other processes on the Br/BrO partitioning (e.g., BrO + NO, IO + BrO) (W. Bloss, personal communication, 2013). To be comparable to our calculations made for DDU, a typical Br mixing ratio was calculated for each site by assuming steady state equilibrium between the BrO photolysis and the reaction of Br with ozone. Finally, at both sites we have assumed a Cl concentration of 2.3×10^3 radicals cm^{-3} as derived by *Read et al*. [2007] for spring at HA from examination of the ethane and propane mixing levels there. At HA we found a weaker sink of HCHO from halogen chemistry (−9 pptv instead of −44 to −82 pptv) than calculated by *Salmon et al*. [2008]. Note that this is almost exclusively driven by the 4 times higher J_{HCHO} value, and not due to the changed Br mixing ratio applied here (0.45 pptv instead of 0.8 pptv, see Table 4). Applying the original value of 0.8 pptv used by *Salmon et al*. [2008] would have resulted in a halogen destruction of −11 pptv instead of −9 pptv calculated here. Consequently, the role of halogen chemistry appears to be more moderate than previously suggested by HA data.

[59] These updated calculations show that the estimated net photochemical budget at HA change from 40 pptv given by *Salmon et al*. [2008] to 36 pptv. This rather small difference is due to the compensation between a far weaker HCHO production from the CH_4 oxidation counterbalanced by a far weaker destruction from halogens in the updated estimation. From that it can be concluded that estimated HCHO mixing ratios related to photochemical sources and sinks are significantly lower in the Weddell Sea sector than that at DDU (30–40 pptv instead of 170 pptv) for January. That is mainly due to a more efficient HO_x chemistry at DDU than at the Weddell Sea site. As seen in Figure 9, calculated photochemical HCHO contributions nearly match observations at DDU in summer but contribute only ~30% (instead of 40% calculated by *Salmon et al*. [2008]) to observed HCHO mixing ratios at HA.

5.2. Snow Emissions in Summer

[60] The snow emissions required at HA to match observations (after having updated gas-phase photochemical calculations as detailed in section 5.1.1) without accounting for deposition processes are 1.15×10^{13} molecule m^{-2} s^{-1} (Table 4). Considering a 100 m BDL height [*Salmon et al*., 2008] and the upper limit of *v* derived for DDU (0.4 cm s^{-1}, see section 4.3.1), a maximal snow flux of 3×10^{13} molecule m^{-2} s^{-1} is required to match observations at HA. However, BDL heights of 40 m to 110 m were deduced from acoustic radar measurements made at HA in 2003 (annual mean of 70 m [*Jones et al*., 2008]). Using the mean value of 70 m, the calculated snow flux is of 2.5×10^{13} molecule m^{-2} s^{-1} (Table 4). Note that in these calculations, a rather well-mixed BDL was assumed given a diffusive mixing time of 3 h (P. Anderson, personal communication, 2013) compared to the mean HCHO lifetime of 4 h.

[61] Considering relevant A and T values for the catchment area of the potential snowpack source at HA (*Arthern et al.* [2006] and data from THERMAP, see section 4.2), we would assume a similar snow emission strength to the one estimated for DDU ($0.5–1 \times 10^{13}$ molecule m^{-2} s^{-1}, see section 4.2). Consistent with that, the value of the snow emission flux needed to match observations at HA is similar to the one derived for DDU; however, both are 2 to 3 times larger than the value predicted on the basis of A and T parameters.

[62] Thus, assuming a deposition velocity of 0.4 cm s^{-1}, HA and DDU measurements suggest HCHO snow emissions ranging between 2×10^{13} and 3×10^{13} molecule m^{-2} s^{-1} in summer. These snow emissions that dominate the HCHO summer budget at the West Antarctic site of HA are, however, less important at DDU (Figure 9). This difference is due to a shallower BDL height at HA compared to DDU as well as to a stronger HCHO production from photochemistry at DDU compared to HA.

6. Summary and Conclusions

[63] A year-round HCHO record was obtained at the coastal East Antarctic site of Dumont d'Urville in 2009 using a commercial HCHO analyzer (Aerolaser, AL-4021). Working conditions were optimized to permit accurate measurements of mixing ratios as low as a few tens of parts per trillion by volume as encountered there in winter. Raw data were carefully cleaned from impact of local contamination sources that exist at the site (combustion related to station activities and release of volatile organic compounds following bacterial decomposition of guano from Adelie penguins). The filtered HCHO record shows a seasonal cycle with monthly mean winter levels close to 50 pptv reaching 200 pptv in January.

[64] HCHO steady state mixing ratio calculated considering loss of HCHO by photolysis and reaction with OH together with gas-phase production from oxidation of methane, ethene, and DMS reproduce fairly well the observations made at DDU in summer when no deposition is considered. The main gas-phase precursor of HCHO is CH_4 due to its efficient oxidation by OH and NO, which is considerably more important than the oxidation of light alkenes and DMS. To match observations, it was necessary to invoke a dry deposition velocity of 0.4 cm s^{-1} and a snow emission close to 2×10^{13} molecule m^{-2} s^{-1}, which is roughly consistent with published estimates. In winter, the local photochemistry is weakened ($< 20\%$) which increases the importance of the contribution of snow emissions (more than 60%), whereas the contribution of long-range transport is found to be rather small ($< 20\%$).

[65] The availability of year-round HCHO records obtained at two different coastal Antarctic sites allowed, for the first time, to draw a conclusive picture of HCHO sources and sinks governing the HCHO budget at these coastal Antarctic regions in summer. While the largest source of HCHO at DDU is the gas-phase photochemistry (80%), HCHO snow emissions dominate at HA (85%). The gas-phase photochemistry at both sites is dominated by the oxidation of methane which is, however, about 3 times more efficient in producing HCHO at DDU than at HA mainly because of more frequent arrival of oxidant-rich air masses, coming from the Antarctic plateau, at DDU. The halogen chemistry remains a weak sink of HCHO at both sites. Although snow emissions are probably of similar strength around the two sites, the shallower atmospheric boundary at HA compared to DDU permits a more efficient accumulation of HCHO emitted by this surface source.

Appendix A1: Sensitivity of AL-4021 Aerolaser Analyzers to Temperature Changes

[66] Since the sensitivity of AL-4021 Aerolaser analyzer to ambient temperature changes (see section 2.1) is not yet documented in the literature but clearly needs to be addressed when measuring low HCHO levels with this device, further investigations were made on the analyzers back at the LGGE in 2010. In the following we report major findings of this study, which are detailed in *Pépy* [2011].

[67] In a first step, key elements (stripping solution and liquid reagent, gas inlet line, stripper, reactor, and fluorimeter/photomultiplier unit) of the AL-4021 were separately exposed to temperature changes to identify which components are sensitive to temperature variations. It turned out that the analyzer is not sensitive to the temperature of sampled air but that the ambient laboratory temperature influences the fluorimeter/photomultiplier unit and the reactor. The response of the fluorimeter/photomultiplier unit appeared to be anticorrelated to temperature changes. This is likely due to the photomultiplier, which becomes more sensitive at lower temperature in relation to a reduction of the background noise level (T. Deparade, Aerolaser company, personal communication, 2013). Conversely, even though it is thermostated, the reactor responds noticeably to fast temperature changes, which arises from a temperature dependence of the Hantzsch reaction efficiency. That is likely due to an inadequate reactor temperature regulation (at ~ 70°C), which is unable to compensate fast temperature changes.

[68] For both effects further investigations were made to evaluate whether the temperature dependency corresponds to a signal offset or to an amplification of the signal. To do so the same air was sampled by an analyzer placed in a climatic chamber and exposed to controlled temperature changes, whereas another one was run at a stable ambient temperature. Zero measurements were made every 2 h on the two analyzers. Slow cyclic variations of ambient temperature with a gradient of 1 to 2°C h^{-1} were first applied to reproduce typical diurnal cycle observed in the DDU laboratory during the 2005 and 2006 pilot studies. These slow temperature changes would affect mainly the fluorimeter/photomultiplier unit, the temperature regulation of the reactor being able to compensate slow temperature changes. As seen in Figure A1, the AL-4021 zero signal is anticorrelated with a slope of −14 mV °C^{-1}, corresponding to −50 pptv of HCHO °C^{-1}. Thus, running the analyzer without regular monitoring of the zero signal at a place where temperature changes can reach 10 to 20°C may induce errors in the range of 250 to 500 pptv of HCHO. The change of the HCHO signal with temperature was found to be independent of the HCHO level of sampled air (mixing ratios ranging from 100 to 1000 pptv during our experiment) since the linear regression of concentrations derived by the two analyzers showed a very linear relationship ($y = 0.97\ x$ and $R^2 = 0.94$). This suggests that this temperature artifact is mainly an offset and not an amplification effect.

[69] To investigate the effect of temperature on the AL-4021 reactor, a high temperature gradient of 6°C h^{-1} was applied,

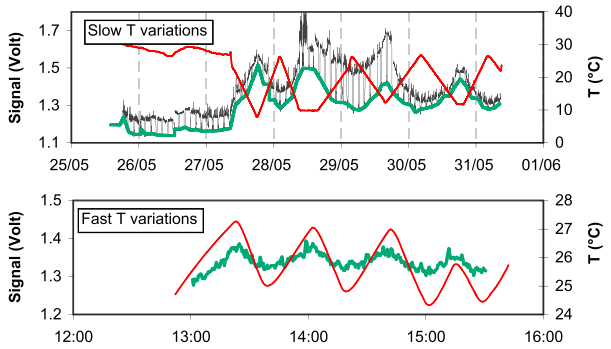

Figure A1. The temperature change effects on the AL-4021 device as observed in a climatic chamber. (top) Signal (thin black line) and zero (green line) records of the analyzer during sampling of HCHO mixing ratios between 100 and 1000 pptv and when a slow temperature gradient (red line) was applied. (bottom) Zero record of the AL-4021 analyzer (green line) when a fast ambient temperature variation (red line) was applied.

inducing a signal variation of +107 pptv $°C^{-1}$ (Figure A1). As for the preceding experiment, the temperature dependency of the signal was found to be independent of the HCHO level. Thus, an abrupt temperature variation (e.g., the opening of the door of the field lab when outside temperatures are 30°C less than inside) of up to ±3°C over a few minutes may enhance the HCHO signal by up to 300 pptv.

Appendix B1: The 2-D Simulation Tool

[70] To compare the impact of gas-phase photochemistry with that from snow emissions coming from the Antarctic continent to the DDU site, gas-phase photochemical sources and sinks from the 0-D calculations were implemented in a 2-D simulation, spanning a vertical transect along 140°E from the coast to inland Antarctica. In addition to snow emission, a dry deposition was considered in the calculations.

[71] A grid of 200 × 5 km horizontal and 15 × 20 m vertical cells was considered on which DDU is situated on the lower right side. Transport mechanisms between the grid cells include diffusion in both directions and horizontal wind transport toward DDU. Vertical and horizontal diffusion is assessed using eddy diffusion coefficients (K_z) calculated by the Modèle Atmosphérique Régional (MAR) [*Gallée et al*., 2012] for the automatic weather station D47 (situated on the Antarctic continent ~110 km away from DDU) over a 10 day period of typical stable continental flow conditions in summer (1–9 January 2010). K_z values vary with height from ~2.5 to ~7 $m^2\ s^{-1}$ from the ground to higher altitudes, reaching maximum value around 180 m. These boundary layer conditions are typical for katabatic conditions at DDU [*Gallée and Pettré*, 1998]. In line with the vertical distribution of K_z values, the upper layer of the 2-D grid was fixed to end at 300 m height. In addition, K_z values show a diurnal cycle with a maximum at the beginning of the afternoon in phase with the daily cycle observed for air and snow temperatures at D47 during this period (data available at http://amrc.ssec.wisc.edu/aws/). Being representative for katabatic conditions, for which air mass is conserved during transport down slope to DDU, we consider the D47 K_z values to be appropriate over the whole horizontal length of the 2-D grid (i.e., over a region of 1000 km inland of DDU). To avoid border effects, a constant HCHO level is attributed at the left vertical border of the grid (i.e., 1000 km inland from DDU). The right vertical grid border side (i.e., at DDU) is kept open with respect to transport mechanisms.

[72] Snow emissions and deposition velocities were applied to the lowest horizontal grid layer. To account for the absence of snow accumulation over the first 20 km inland of DDU (see section 4.2), the snow flux is set to zero in the four left hand adjacent grids of DDU.

[73] To constrain the daily HCHO variation observed in summer at DDU, the 2-D model was run in hourly resolution using January conditions. Temperature, diffusion rates, photolytic rates, OH, and NO levels were assumed to vary over the course of the day. While diffusion coefficients and inputs for photolytic rate estimations were taken from the respective models (see above and section 4.1.1), the daily cycle of OH is taken from OH measurements [*Kukui et al*. 2012] and the one of NO from *Grilli et al*. [2013]. Daily variations of wind speeds and diffusive transport velocities, as well as variable HCHO lifetimes (~ 3 and ~ 15 h at night and day, respectively) may influence the impact of a nonconstant snow flux on the daily course of HCHO mixing ratios at DDU. Therefore, a series of 2-D model runs including constant (between 6 and 14 $m\ s^{-1}$) and daily variable wind speed patterns (i.e., with a minimum during midday as observed at DDU and D47 under stable katabatic conditions in summer) were done. No significant differences were, however, observed for the calculated HCHO levels in the DDU model grid, which is attributed to the relatively strong K_z values prevailing inland of DDU and which permits the diffusive equilibrium over the whole BDL depth to be reached within only a few hours (i.e., ~ 3 and 10 h during day and night, respectively). Therefore, we assume that snow emissions from the continent reach DDU without distortion during summer, at least for wind speeds higher than 6 $m\ s^{-1}$. Thus, we used a constant horizontal wind speed of 13 $m\ s^{-1}$ for the 2-D calculations. In daily simulations a variable snow emission source was assumed with an adjustment made on the diurnal temperature cycle of air and snow and assuming zero snow emissions at night.

[74] Concerning the dry deposition of HCHO on ice, under the wind and temperature conditions encountered, and considering a typical surface roughness of 10^{-4} m, the dominant resistances of the deposition velocity (v) are the aerodynamic (Ra) and surface (Rc) ones [*Riedel*, 2001; *Zhang et al*., 2003]. Ra depends inversely on the friction velocity (u^*) and Rc inversely on temperature over the range of −5 to +0.6°C [*Zhang et al*., 2003; *Erisman et al*., 1994], respectively. Conditions encountered at different distances inland from DDU were checked using u^* and meteorological data from the MAR model (see above) and from automatic weather stations data (available at http://amrc.ssec.wisc.edu/aws). It can be concluded that over the continent near DDU at midday, a systematic minimum of u^*, which is driven by the wind speed, generally coincides with the simultaneous temperature maximum, resulting in a rather unchanged value of v over the course of the day. Further inland, wind speed and u^* show no significant daily variation anymore, and the night and day temperatures are both too low to influence the surface resistance anymore. Thus, the dry deposition

was assumed to be constant over day and night in our calculations. Applying these parameterizations of Ra and Rc for our conditions, a mean v value of 0.2 ± 0.04 is obtained. For winter, the aerodynamic resistance (Ra) is found to be similar to the one calculated for summer, since the average wind speed value of 10 m s^{-1} inland of DDU is rather similar in summer and winter. In contrast to the summer period, when a temperature exceeding over −5°C is possible in a very limited coastal area around DDU, temperatures remain everywhere (at DDU as well as on the continent) well below −5° C in winter. Therefore, we assume that the mean surface resistance (Rc) remains equal or only slightly higher in winter than in summer. As a consequence, compared to summer only slightly lower or even unchanged deposition velocities are expected in winter inland of DDU.

[75] Considering exclusively snow emission and deposition, as done for winter conditions, makes the calculations in principle independent of the BDL height. However, the region without snow flux (20 km adjacent inland of DDU) induces the BDL height to influence calculated HCHO mixing ratios at DDU at low horizontal wind speeds. At a wind speed of 1 m s^{-1}, a lowering of the BDL height by a factor of 3 would imply 20% lower HCHO calculated levels at DDU. This effect becomes, however, less than 5% and 1% for wind speeds higher than 1.5 and 2 m s^{-1}, respectively. Since the wind speed at DDU is higher than 2 m s^{-1} for 85% of continental winter conditions, this transport effect was neglected.

[76] **Acknowledgments.** National financial support and field logistic supplies were provided by Institut Polaire Français-Paul Emile Victor (IPEV) within program N° 414. This work was also partly funded by the Centre National de la Recherche Scientifique (INSU) and the OPALE project supported by the ANR (Agence National de Recherche, contract ANR-09-BLAN-0226). The authors thank Andrea Pazmino (LATMOS, CNRS) for providing the UVB data and Meteo France for global irradiance and other basic meteorological parameters. Thanks to the Natural Environment Research Council (NERC) for the open access to the CHABLIS data, to Bill Bloss and Phil Anderson for useful discussions. Likewise, thanks a lot to Katja Riedel and Rolf Weller for discussions on NM data and to Tobias Deparade from AEROLASER company for providing useful technical details on the AL-4021 analyzer. The authors gratefully acknowledge the NOAA Air Resources Laboratory (ARL) for the availability of the HYSPLIT model. Thanks also to the Chemical Processing and Regional Modeling research group (CPRM) of the National Center of Atmospheric Research (NCAR) for the open accessibility of their Tropospheric Ultraviolet and Visible radiative transfer column model. Thanks to the Global Monitoring Division of the Earth System Research Laboratory (ESRL) for the open access to CH_4 data from Syowa Station. SAOZ data used in this publication were obtained as part of the Network for the Detection of Atmospheric Composition Change (NDACC) available at http://www.ndacc.org. Thanks to the Physical Sciences Division of the NOAA/OAR/ESRL PSD, Boulder, Colorado, USA, for NOAA_OI_SST_V2 sea ice data. The authors appreciate the support of the Automatic Weather Station Program of AMRC, SSEC, and UW-Madison. Thanks to the THERMAP research team of National Snow and Ice Data Center (NSIDC) CIRES, 449 UCB University of Colorado, Boulder, for giving open access to annual mean temperature data over the Antarctic ice sheet.

References

Agosta, C., V. Favier, C. Genthon, H. Gallée, G. Krinner, J. T. M. Lenaerts, and M. R. van den Broeke (2011), A 40-year accumulation dataset for Adelie Land Antarctica and its application for model validation, *Clim. Dyn.*, doi:10.1007/s00382-011-1103-4.

Arthern, R. J., D. P. Winebrenner, and D. G. Vaughan (2006), Antarctic snow accumulation mapped using polarization of 4.3-cm wavelength microwave emission, *J. Geophys. Res.*, *111*, D06107, doi:10.1029/2004JD005667.

Atkinson, R., D. L. Baulch, R. A. Cox, J. N. Crowley, R. F. Hampson, R. G. Hynes, M. E. Jenkin, M. J. Rossi, and J. Troe (2004), Evaluated kinetic and photochemical data for atmospheric chemistry: Volume I—Gas phase reactions of Ox, HOx, NOx and SOx species, *Atmos. Chem. Phys.*, *4*(6), 1,461–1,738, doi:10.5194/acp-4-1461-2004.

Atkinson, R., D. L. Baulch, R. A. Cox, J. N. Crowley, R. F. Hampson, R. G. Hynes, M. E. Jenkin, M. J. Rossi, J. Troe, and I. U. P. A. C. Subcommittee (2006), Evaluated kinetic and photochemical data for atmospheric chemistry: Volume II—Gas phase reactions of organic species, *Atmos. Chem. Phys.*, *6*(11), 3625–4055, doi:10.5194/acp-6-3625-2006.

Atkinson, R., D. L. Baulch, R. A. Cox, J. N. Crowley, R. F. Hampson, R. G. Hynes, M. E. Jenkin, M. J. Rossi, and J. Troe (2007), Evaluated kinetic and photochemical data for atmospheric chemistry: Volume III—Gas phase reactions of inorganic halogens, *Atmos. Chem. Phys.*, *7*(4), 981–1191, doi:10.5194/acp-7-981-2007.

Atkinson, R., D. L. Baulch, R. A. Cox, J. N. Crowley, R. F. Hampson, R. G. Hynes, M. E. Jenkin, M. J. Rossi, J. Troe, and T. J. Wallington (2008), Evaluated kinetic and photochemical data for atmospheric chemistry: Volume IV—Gas phase reactions of organic halogen species, *Atmos. Chem. Phys.*, *8*(15), 4141–4496, doi:10.5194/acp-8-4141-2008.

Ayers, G. P., R. W. Gillett, H. Granek, C. de Serves, and R. A. Cox (1997), Formaldehyde production in clean marine air, *Geophys. Res. Lett.*, *24*(4), 401–404, doi:10.1029/97GL00123.

Barret, M., S. Houdier, and F. Domine (2011), Thermodynamics of the Formaldehyde—Water and Formaldehyde—Ice Systems for Atmospheric Applications, *J. Phys. Chem. A*, *115*(3), 307–317, doi:10.1021/jp108907u.

Bloomfield, F., and W. L. Steiger (1983), *Least Absolute Deviations: Theory, Applications, and Algorithms*, Birkhauser, Boston, Mass, USA.

Bloss, W. J., J. D. Lee, D. E. Heard, R. A. Salmon, S. J.-B. Bauguitte, H. K. Roscoe, and A. E. Jones (2007), Observations of OH and HO_2 radicals in coastal Antarctica, *Atmos. Chem. Phys.*, *7*(16), 4171–4185, doi:10.5194/acp-7-4171-2007.

Carslaw, N., P. J. Jacobs, and M. J. Pilling (1999), Modeling OH, HO_2, and RO_2 radicals in the marine boundary layer 2. Mechanism reduction and uncertainty analysis, *J. Geophys. Res.*, *104*(D23), 30,257–30,273.

Chen, G., et al. (2004), A reassessment of HOx South Pole chemistry based on observations recorded during ISCAT 2000, *Atmos. Environ.*, *38*(32), 5451–5461, doi:10.1016/j.atmosenv.2003.07.018.

Dasgupta, P. K., S. Dong, H. Hwang, H.-C. Yang, and Z. Genfa (1988), Continuous liquid-phase fluorometry coupled to a diffusion scrubber for the real-time determination of atmospheric formaldehyde, hydrogen peroxide and sulfur dioxide, *Atmos. Environ.*, *22*(5), 949–963, doi:10.1016/0004-6981(88)90273-9.

Davis, D., et al. (2001), Unexpected high levels of NO observed at South Pole, *Geophys. Res. Lett.*, *28*(19), 3625–3628, doi:10.1029/2000GL012584.

DeMore, W. B., S. P. Sander, D. M. Golden, R. F. Hampson, M. J. Kurylo, C. J. Howard, A. R. Ravishankara, C. E. Kolb, and M. J. Molina (1997), Chemical kinetics and photochemical data for use in stratospheric modeling, Evaluation 12, JPL Publ., 97–4.

Erisman, J. W., A. Van Pul, and G. P. Wyers (1994), Parameterization of surface resistance for the quantification of atmospheric deposition of acidifying pollutants and ozone, *Atmos. Environ.*, *28*, 2595–2607.

Ervens, B., G. Feingold, G. J. Frost, and S. M. Kreidenweis (2004), A modeling study of aqueous production of dicarboxylic acids: 1. Chemical pathways and speciated organic mass production, *J. Geophys. Res.*, *109*, D15205, doi:10.1029/2003JD004387.

Frey, M. M., R. W. Stewart, J. R. McConnell, and R. C. Bales (2005), Atmospheric hydroperoxides in West Antarctica: Links to stratospheric ozone and atmospheric oxidation capacity, *J. Geophys. Res.*, *110*, D23301, doi:10.1029/2005JD006110.

Gallée, H., and P. Pettré (1998), Dynamical constraints on katabatic wind cessation in Adélie Land, Antarctica, *J. Atmos. Sci.*, *55*(10), 1755–1770.

Gallée, H., A. Trouvilliez, C. Agosta, C. Genthon, V. Favier, and F. Naaim (2012), Transport of snow by the wind: A comparison between observations made in Adélie Land Antarctica, and simulations made with the Regional Climate Model MAR, *Boundary Layer Meteorol.*, *146*, 133–147, doi:10.1007/s10546-012-9764-z.

Grilli, R., M. Legrand, A. Kukui, G. Méjean, S. Preunkert, and D. Romanini (2013), First investigations of IO, BrO, and NO_2 summer atmospheric levels at a coastal East Antarctic site using mode-locked cavity enhanced absorption spectroscopy, *Geophys. Res. Lett.*, *40*, 1–6, doi:10.1002/grl.50154.

Grutter, M., E. Flores, G. Andraca-Ayala, and A. Baez (2005), Formaldehyde levels in downtown Mexico City during 2003, *Atmos. Environ.*, *39*(6), 1027–1034, doi:10.1016/j.atmosenv.2004.10.031.

Hauptmann, M., J. H. Lubin, P. A. Stewart, R. B. Hayes, and A. Blair (2003), Mortality from lymphohematopoietic malignancies among workers in formaldehyde industries, *J. Natl. Cancer Inst.*, *95*(21), 1615–1623, doi:10.1093/jnci/djg083.

Hutterli, M. A., R. Rothlisberger, and R. C. Bales (1999), Atmosphere-to-snow-to-firn transfer studies of HCHO at Summit, Greenland, *Geophys. Res. Lett.*, *26*(12), 1691–1694, doi:10.1029/1999GL900327.

Hutterli, M. A., J. R. McConnell, R. C. Bales, and R. W. Stewart (2003), Sensitivity of hydrogen peroxide (H_2O_2) and formaldehyde (HCHO)

preservation in snow to changing environmental conditions: Implications for ice core records, *J. Geophys. Res.*, *108*(D1), 4023, doi:10.1029/2002JD002528.

Hutterli, M. A., J. R. McConnell, G. Chen, R. C. Bales, D. D. Davis, and D. H. Lenschow (2004), Formaldehyde and hydrogen peroxide in air, snow and interstitial air at South Pole, *Atmos. Environ.*, *38*(32), 5439–5450.

Jacobi, H. W., M. M. Frey, M. A. Hutterli, R. C. Bales, O. Schrems, N. J. Cullen, K. Steffen, and C. Koehler (2002), Measurements of hydrogen peroxide and formaldehyde exchange between the atmosphere and surface snow at Summit, Greenland, *Atmos. Environ.*, *36*(15–16), 2619–2628.

Jefferson, A., D. J. Tanner, F. L. Eisele, D. D. Davis, G. Chen, J. Crawford, J. W. Huey, A. L. Torres, and H. Berresheim (1998), OH photochemistry and methane sulfonic acid formation in the coastal Antarctic boundary layer, *J. Geophys. Res.*, *103*(D1), 1647–1656, doi:10.1029/97JD02376.

Jones, A. E., et al. (2008), Chemistry of the Antarctic boundary layer and the interface with snow: An overview of the CHABLIS campaign, *Atmos. Chem. Phys.*, *8*(14), 3789–3803.

Jourdain, B., and M. Legrand (2001), Seasonal variations of atmospheric dimethylsulfide, dimethylsulfoxide, sulfur dioxide, methanesulfonate, and non-sea-salt sulfate aerosols at Dumont d'Urville (coastal Antarctica) (December 1998 to July 1999), *J. Geophys. Res.*, *106*(D13), 14,391–14,408, doi:10.1029/2000JD900841.

König-Langlo, G., J. C. King, and P. Pettré (1998), Climatology of the three coastal Antarctic stations Dumont d'Urville, Neumayer, and Halley, *J. Geophys. Res.*, *103*(D9), 10,935–10,946, doi:10.1029/97JD00527.

Kukui, A., M. Legrand, G. Ancellet, V. Gros, S. Bekki, R. Sarda-Estève, R. Loisil, and S. Preunkert (2012), Measurements of OH and RO_2 radicals at the coastal Antarctic site of Dumont d'Urville (East Antarctica) in summer, *J. Geophys. Res.*, *117*, D12310, doi:10.1029/2012JD017614.

Legrand, M., S. Preunkert, B. Jourdain, H. Gallée, F. Goutail, R. Weller, and J. Savarino (2009), Year-round record of surface ozone at coastal (Dumont d'Urville) and inland (Concordia) sites in East Antarctica, *J. Geophys. Res.*, *114*, D20306, doi:10.1029/2008JD011667.

Legrand, M., V. Gros, S. Preunkert, R. Sarda-Estève, A.-M. Thierry, G. Pépy, and B. Jourdain (2012), A reassessment of the budget of formic and acetic acids in the boundary layer at Dumont d'Urville (coastal Antarctica): The role of penguin emissions on the budget of several oxygenated volatile organic compounds, *J. Geophys. Res.*, *117*, D06308, doi:10.1029/2011JD017102.

Limbert, D. W. S. (1963), The snow accumulation budget at Halley Bay in 1959, and associated meteorological factors, *Br. Antarct. Surv. Bull.*, *2*, 73–92.

Lowe, D. C., and U. Schmidt (1983), Formaldehyde (HCHO) measurements in the Nonurban Atmosphere, *J. Geophys. Res.*, *88*(C15), 10,844–10,858, doi:10.1029/JC088iC15p10844.

Madronich, S., and S. Flocke (1998), in *The Role of Solar Radiation in Atmospheric Chemistry*, Handbook of Environmental Chemistry, edited by P. Boule, pp. 1–26, Springer, New York.

Mauldin, I. R. L., E. Kosciuch, B. Henry, F. L. Eisele, R. Shetter, B. Lefer, G. Chen, D. Davis, G. Huey, and D. Tanner (2004), Measurements of OH, HO_2+ RO_2, H_2SO_4, and MSA at the South Pole during ISCAT 2000, *Atmos. Environ.*, *38*(32), 5423–5437.

Michalowski, B. A., J. S. Francisco, S.-M. Li, L. A. Barrie, J. W. Bottenheim, and P. B. Shepson (2000), A computer model study of multiphase chemistry in the Arctic boundary layer during polar sunrise, *J. Geophys. Res.*, *105*(D12), 145.

Müller, J.-F., and G. Brasseur (1995), IMAGES: A three-dimensional chemical transport model of the global troposphere, *J. Geophys. Res.*, *100*(D8), 16,445–16,490, doi:10.1029/94JD03254.

Nash, T. (1953), The colorimetric estimation of formaldehyde by means of the Hantzsch reaction, *Biochem. J.*, *55*(3), 416–421.

Niki, H., P. D. Maker, C. M. Savage, and L. P. Breitenbach (1981), An FTIR study of mechanisms for the HO radical initiated oxidation of C_2H_4 in the presence of NO: Detection of glycolaldehyde, *Chem. Phys. Lett.*, *80*, 499–503.

Pépy, G. (2011), Etude du formaldéhyde (HCHO) en zone côtière Antarctique, PhD thesis, 251 pp., Univ. Joseph Fourier de Grenoble, Grenoble, France.

Preunkert, S., G. Ancellet, M. Legrand, A. Kukui, M. Kerbrat, R. Sarda-Estève, V. Gros, and B. Jourdain (2012), Oxidant production over Antarctic land and its export (OPALE) project: An overview of the 2010–2011 summer campaign, *J. Geophys. Res.*, *117*, D15307, doi:10.1029/2011JD017145.

Read, K., A. C. Lewis, R. A. Salmon, A. E. Jones, and S. J. B. Bauguitte (2007), OH and halogen atom influence on the variability of non-methane hydrocarbons in the Antarctic Boundary Layer, *Tellus B*, *59*(1), 22–38, doi:10.1111/j.1600-0889.2006.00227.x.

Riedel, K. (2001), Investigation of the photooxidants hydrogen peroxide, methylhydroperoxide, and formaldehyde in the troposphere of Antarctica, PhD thesis., pp. 157, Alfred-Wegener-Institut für Polar- und Meeresforschung.

Riedel, K., R. Weller, and O. Schrems (1999), Variability of formaldehyde in the Antarctic troposphere, *Phys. Chem. Chem. Phys.*, *1*(24), 5523–5527.

Riedel, K., R. Weller, O. Schrems, and G. König-Langlo (2000), Variability of tropospheric hydroperoxides at a coastal surface site in Antarctica, *Atmos. Environ.*, *34*(29–30), 5225–5234.

Saiz-Lopez, A., A. S. Mahajan, R. A. Salmon, S. J.-B. Bauguitte, A. E. Jones, H. K. Roscoe, and J. M. C. Plane (2007), Boundary layer halogens in coastal Antarctica, *Science*, *317*(5836), 348–351, doi:10.1126/science.1141408.

Salmon, R. A., S. J.-B. Bauguitte, W. Bloss, M. A. Hutterli, A. E. Jones, K. Read, and E. W. Wolff (2008), Measurement and interpretation of gas-phase formaldehyde concentrations obtained during the CHABLIS campaign in coastal Antarctica, *Atmos. Chem. Phys.*, *8*(14), 4085–4093, doi:10.5194/acp-8-4085-2008.

Sciare, J., N. Mihalopoulos, and F. Dentener (2000), Interannual variability of atmospheric dimethylsulfide in the southern Indian Ocean, *J. Geophys. Res.*, *105*, 26,369–26,377.

Stavrakou, T., J.-F. Müller, I. De Smedt, M. Van Roozendael, G. R. van der Werf, L. Giglio, and A. Guenther (2009), Evaluating the performance of pyrogenic and biogenic emission inventories against one decade of space-based formaldehyde columns, *Atmos. Chem. Phys.*, *9*(3), 1037–1060, doi:10.5194/acp-9-1037-2009.

Sumner, A. L., and P. B. Shepson (1999), Snowpack production of formaldehyde and its effect on the Arctic troposphere, *Nature*, *398*, 230–233, doi:10.1038/18423.

Theys, N., et al. (2011), Global observations of tropospheric BrO columns using GOME-2 satellite data, *Atmos. Chem. Phys.*, *11*(4), 1791–1811.

Wagner, V., C. Schiller, and H. Fischer (2001), Formaldehyde measurements in the marine boundary layer of the Indian Ocean during the 1999 INDOEX cruise of the R/V Ronald H. Brown, *J. Geophys. Res.*, *106*(D22), 28,529–28,538, doi:10.1029/2000JD900825.

Wagner, V., R. von Glasow, H. Fischer, and P. J. Crutzen (2002), Are CH_2O measurements in the marine boundary layer suitable for testing the current understanding of CH_4 photooxidation?: A model study, *J. Geophys. Res.*, *107*(D3), 4029, doi:10.1029/2001JD000722.

Weller, R., A. E. Jones, A. Wille, H. W. Jacobi, H. P. McIntyre, W. T. Sturges, M. Huke, and D. Wagenbach (2002), Seasonality of reactive nitrogen oxides (NO_y) at Neumayer Station, Antarctica, *J. Geophys. Res.*, *107*(D23), 4673, doi:10.1029/2002JD002495.

Wisthaler, A., et al. (2008), Technical note: Intercomparison of formaldehyde measurements at the atmosphere simulation chamber SAPHIR, *Atmos. Chem. Phys.*, *8*(8), 2189–2200.

Wittrock, F., A. Richter, H. Oetjen, J. P. Burrows, M. Kanakidou, S. Myriokefalitakis, R. Volkamer, S. Beirle, U. Platt, and T. Wagner (2006), Simultaneous global observations of glyoxal and formaldehyde from space, *Geophys. Res. Lett.*, *33*, L16804, doi:10.1029/2006GL026310.

Yang, J., R. E. Honrath, M. C. Peterson, J. E. Dibb, A. L. Sumner, P. B. Shepson, M. Frey, H.-W. Jacobi, A. Swanson, and N. Blake (2002), Impacts of snowpack emissions on deduced levels of OH and peroxy radicals at Summit, Greenland, *Atmos. Environ.*, *36*(15–16), 2523–2534.

Yin, F., D. Grosjean, and J. H. Seinfeld (1990), Photooxidation of dimethyl sulfide and dimethyl disulfide. I: Mechanism development, *J. Atmos. Chem.*, *11*(4), 309–364.

Zhang, L., J. R. Brook, and R. Vet (2003), A revised parameterization for gaseous dry deposition in air-quality models, *Atmos. Chem. Phys.*, *3*(6), 2067–2082.